Journal of the Geological Society

The mafic alkaline volcanism of SW Madagascar (Ankililoaka, Tulear region): 40Ar/39Ar ages, geochemistry and tectonic setting

--Manuscript Draft--

Manuscript Number:	jgs2017-139
Article Type:	Research article
Full Title:	The mafic alkaline volcanism of SW Madagascar (Ankililoaka, Tulear region): 40Ar/39Ar ages, geochemistry and tectonic setting
Short Title:	Cenozoic mafic alkaline volcanism of SW Madagascar
Corresponding Author:	ciro cucciniello Universita degli Studi di Napoli Federico II ITALY
Corresponding Author E-Mail:	ciro.cucciniello@unina.it
Other Authors:	Anton le Roex
	Fred Jourdan
	Vincenzo Morra
	Celestino Grifa
	Luigi Franciosi
	Leone Melluso
Manuscript Classifications:	Dating (radiometric, absolute, etc); Geochemistry; Magmatic studies
Additional Information:	
Question	**Response**
Are there any conflicting interests, financial or otherwise?	No
Samples used for data or illustrations in this article have been collected in a responsible manner	Confirmed
Suggested Reviewers:	Michael Storey Natural History Museum of Denmark michael.storey@snm.ku.dk expert in geochronology and geochemistry
	Andy Saunders University of Leicester ads@leicester.ac.uk expert in geochemistry and large igneous provinces (e.g., Madagascar continental flood basalt)
Opposed Reviewers:	

Author cover letter

Dr. C. Cucciniello
Dipartimento di Scienze della Terra, dell'Ambiente e delle Risorse (DiSTAR) Università di Napoli Federico II, Italy
e-mail: ciro.cucciniello@unina.it

November 22, 2017

To the Editor of Journal of the Geological Society

Dear Editor,

I would appreciate your considering the enclosed manuscript for publication in *Journal of the Geological Society*

Title: **The mafic alkaline volcanism of SW Madagascar (Ankililoaka, Tulear region): ^{40}Ar/^{39}Ar ages, geochemistry and tectonic setting**

Authors: C. Cucciniello, A.P. le Roex, F. Jourdan, V. Morra, C. Grifa, L. Franciosi, L. Melluso

This manuscript concerns on a volumetrically small monogenetic volcanic field located in southwestern Madagascar (Ankililoaka district). A detailed geochemical, mineralogical and isotopic study has been carried out, with mineral chemical, and whole-rock geochemical (elemental and Nd-Sr-Pb isotopic) data, as well as Ar-Ar geochronolgy on several samples collected in this area. We propose a petrogenetic model for the genesis of the alkaline mafic rocks and point out the similarities of these rocks with those found in the other Cenozoic districts of northernmost Madagascar. The manuscript has not been published previously, and is not under consideration for publication elsewhere.

I look forward to hearing from you, and thank you for considering our manuscript.

Sincerely yours,

Ciro Cucciniello

The mafic alkaline volcanism of SW Madagascar (Ankililoaka, Tulear region): $^{40}Ar/^{39}Ar$ ages, geochemistry and tectonic setting

C. Cucciniello[1*], A.P. le Roex[2], F. Jourdan[3], V. Morra[1], C. Grifa[4], L. Franciosi[1], L. Melluso[1]

[1] DiSTAR Università di Napoli Federico II, Italy
[2] University of Cape Town, RSA
[3] Curtin University, Australia
[4] Università del Sannio, Italy
*Corresponding author (ciro.cucciniello@unina.it)

Abstract

New high-precision $^{40}Ar/^{39}Ar$ ages, major, trace element and radiogenic isotope data are presented for basanites and alkali basalts of a monogenetic volcanic area located in southwestern Madagascar (Ankililoaka, Tulear region). The volcanic rocks were erupted along fissure zones and aligned cones in a nearly flat area covered by Cenozoic sediments of the Morondava basin. The $^{40}Ar/^{39}Ar$ determinations yield ages of ~11-12 Ma, distinctly different from previous K-Ar ages, indicating a short time span that significantly overlaps with ages of other volcanic rocks in northern and central Madagascar. The Ankililoaka basanites include primitive compositions (MgO > 10 wt.%, Ni > 200 ppm and Cr > 400 ppm), whereas other basanites and alkali basalts experienced limited removal of olivine, chromiferous spinel and clinopyroxene. The Ankililoaka basanites and alkali basalts are highly enriched in the most incompatible elements, with peaks at Nb, troughs at K, Pb and smooth, decreasing patterns towards the least incompatible elements in the primitive mantle-normalized diagrams. Initial (at 11 Ma) Sr and Nd isotope ratios of Ankililoaka basanites are 0.70343-0.70445 and 0.512792-0.512822, respectively. The Pb isotope compositions are in the ranges $^{206}Pb/^{204}Pb$ = 19.079-19.388, $^{207}Pb/^{204}Pb$ = 15.612-15.640 and $^{208}Pb/^{204}Pb$ = 39.108-39.427. The alkali basalts have similar $^{87}Sr/^{86}Sr$, $^{143}Nd/^{144}Nd$ and $^{207}Pb/^{204}Pb$ but slightly lower $^{206}Pb/^{204}Pb$ and $^{208}Pb/^{204}Pb$ than the basanites. The isotopic composition of

Ankililoaka rocks partially overlaps with that of the Cenozoic volcanic mafic rocks of northern Madagascar, whereas differs markedly from the mafic volcanic rocks of central Madagascar, which have lower $^{206}Pb/^{204}Pb$, $^{207}Pb/^{204}Pb$ and $^{87}Sr/^{86}Sr$. Major and trace element systematics and geochemical modelling suggest that the Ankililoaka mafic alkaline rocks are low-degree melts of an incompatible-element enriched peridotite source starting from depths where garnet is stable. Crustal contamination during ascent was insignificant. We argue that the melting event that generated the Ankililoaka alkaline magmas was triggered by lithospheric thinning related to the uplift of central Madagascar, rather than deep-seated plume-related magmatism, for which there is no geochemical or geophysical evidence.

Keywords: $^{40}Ar/^{39}Ar$ ages; geochemistry; mafic volcanic rocks; mantle sources; Madagascar

Supplementary material: X-ray fluorescence whole rock data, mineral compositions, $^{40}Ar/^{39}Ar$ dataset and mantle source modelling is available at https://doi.org/xxxx

1. Introduction

The study of mafic alkaline volcanic rocks erupted in continental within-plate settings is very useful in highlighting the role of mantle source components and mantle enrichment processes, as well as to establish the actual and fossile tectonic setting of an area. Of importance is the understanding of relationships between the geochemistry of the erupted mafic magmas and the evolution of the mantle source in time and space (the voluminous alkaline magmatism of the East African Rift System is a typical example). In this context, the Cenozoic volcanism is characterized by large amount of ultramafic-mafic mantle-derived rocks (ranging from olivine melilitites to tholeiitic basalts) emplaced at different ages, in both cratonized domains and mobile belts of a Precambrian basement of Archean to Late Proterozoic age and Paleozoic to Recent sedimentary basins.

The Cenozoic volcanic rocks that occur in the northern part of the island (Fig. 1) form very large volcanic complexes (the Massif d'Ambre) and scattered dyke swarms (Cap d'Ambre; Cucciniello *et al*. 2011; Melluso *et al.* 2007). In the Ampasindava area, volcanic fields are present with dyke swarms and often large plutonic intrusions, still partially known and sometimes interesting for REE mineralization (Lacroix 1922, 1923; Melluso & Morra 2000; Cucciniello *et al*. 2016 and references therein; Estrade *et al.* 2014). In the center of the island, scattered lavas crop out in the Alaotra graben and along the eastern coast (Melluso *et al.* 2011b), whereas the Ankaratra complex (*c*. 3800 km^2) is a polyphasic volcanic area, active at least from Miocene to the Quaternary (Cucciniello et *al.* 2017 and references therein); the Itasy is a smaller, mostly Quaternary, monogenetic volcanic field (Battistini 1962; Melluso *et al*. 2007*b*; Fig. 1). Limited outliers are located in the southwest, close to Tulear, and south of Morondava (Nicollet 1984; Fig. 1a). It is not unlikely that further occurrences are yet to be exposed by erosion. The compositional range of these rocks range from olivine melilitites and olivine nephelinites through basanites and basalts to rhyolites, trachytes and phonolites, with a very large geochemical and isotopic variations in both mafic/ultramafic and felsic rocks which are linked to different mantle sources, degree of partial melting and extensive open-system fractional crystallization processes (cf. data and interpretations of Melluso *et al*. 2016; Cucciniello *et al*. 2016 and references therein).

This work is focused on a very peculiar and isulated monogenetic volcanic field located in southwestern Madagascar, the Ankililoaka district (a.k.a. Betioky Nord; Fig. 1). The most significant descriptions of the Ankililoaka volcanic field are reported in the official geological maps, which provide a broad Cenozoic age based on the stratigraphic position of the volcanic centers, and in the work of Nicollet (1984), who also published the major element analysis of a basanite. In this paper, we present a brief volcanological outline, and high precision $^{40}Ar/^{39}Ar$ ages, mineral chemistry, major, trace elements and Sr-Nd-Pb isotope data, which are significantly different from that already published on these rocks (cf. Bardintzeff *et al*. 2010). We propose a petrogenetic model for the genesis of the alkaline mafic rocks and point out similarities and differences between these rocks and those found in other Cenozoic districts of Madagascar.

2. Geological setting

The geology of southwestern Madagascar (exemplified in Fig. 1*a*) is characterized by different tectonic units of Precambrian age and a Meso-Cenozoic sedimentary cover. The Vohibory domain (the most westerly basement domain of southern Madagascar) consists of mafic and felsic orthogneisses of metaophiolitic origin (Jöns & Schenk 2008), which are intercalated with low-Al paragneisses and marbles (Tucker *et al*. 2014 and references therein). The Androyan domain is characterized by biotite–hornblende, biotite-sillimanite-garnet and graphite-sillimanite paragneisses, pyroxene–hornblende ± garnet gneisses and quartz-feldspathic gneisses. The Anosyan domain (the most extensive tectonic unit of southern Madagascar) consists of charnockites, biotite-garnet granites, marbles, pyroxene-scapolite gneisses and cordierite-garnet paragneisses (de Wit *et al*. 2001). The sedimentary cover of the Precambrian basement of southern Madagascar forms bulk of the Morondava basin (Fig. 1*a, b*). It is composed by a thick sedimentary sequence ranging in age from Carboniferous to the Late Triassic belonging to the Karoo Supergroup (mainly fluvial and fluvio-lacustrine deposits; Piqué *et al*. 1999) and from Middle Jurassic to Cenozoic (mainly shallow marine environment; Piqué *et al*. 1999). The Cretaceous rocks (mostly limestones in the Morondava basin) are also intercalated with a limited thickness of flood basalts (Fig. 1*b*); further east, the Ejeda-Bekily dyke swarm cross-cuts the Precambrian basement (Nicollet 1984; Dostal *et al*. 1992).

Madagascar was involved in tectonic processes since the Early Cenozoic (e.g. Piqué *et al*. 1999). Evidence of these processes is provided by the uplift of the central backbone of the island, and the development of several graben or half-graben systems, such as that of Moramanga-Alaotra, the southern part of the Ankaratra region, and the Nosy-Be-Antongil system (Fig. 1*a*). Many or most of these systems have volcanic rocks within, or along their borders (cf. Nicollet 1984;

Melluso *et al*. 2011*a*; Cucciniello *et al*. 2010, 2016, 2017). The crustal thickness of southwestern Madagascar is estimated to be between 20 and 30 km (Rindraharisaona *et al*. 2017).

3. Volcanological setting and sampling sites

The Ankililoaka district is located on the southwestern edge of the Morondava basin, in SW Madagascar (Figs. 1 and 2). It comprises a cluster of plugs, scoria/spatter cones and lava flows, scattered over an area of approximately 400 km^2. In this area, eruption centres ranging from a few hundreds of meters up to few kilometres wide, are present. Particularly evident are five scoria/spatter cones just west of the Betioky village that are tightly aligned along a fracture oriented N18°E running parallel to the regional faulting (cf. Nicollet 1984). These cones still preserve very proximal, subaerial features such as breadcrust and spindle-shaped volcanic bombs (Fig. 3). Other isolated spatter cones in the plain are blocky, or rounded remnants of necks with columnar jointing (Fig. 3). The westernmost outcrop (Ambohitra) is represented by a 400 m- large circular area rich in scoria, bombs and lava fragments (adjacent to the Mikea National Park, roughly 15 km west of the closest outcrops). South of Ampihamy, at 5 km-long lava flow forms the largest outcrop in the area, with its emission centre still evident from the presence of a depressed structure and associated dykes (Fig. 3). The volcanic area is cross-cut by a long regional fault oblique to the alignment of the Betioky cones (the Tulear fault; Fig. 2), that may have had a role in the north-south movements of Madagascar in the Cretaceous, and in the opening of the Mozambique Basin (cf. Phethean *et al*. 2017). This extensional fault system seems to be linked only generally to the tectonics in the Mozambique Basin, located to the west (Phethean *et al*. 2017).

4. Petrography, Classification, Mineral chemistry

The Ankililoaka samples are generally mildly porphyritic, and have phenocrysts of olivine (± chromiferous spinel), or olivine and clinopyroxene (supplementary Fig. 1, available in the online Supplementary materials at https://doi.org/xxxx). Olivine is rare in the groundmass. Plagioclase, clinopyroxene, Fe-Ti oxides and apatite are the most common groundmass phases, and the interstices of the holocrystalline samples also have alkali feldspar, nepheline and sodalite. Rare glass and hydrous phases (biotite and amphibole), sulfides, other accessories and secondary phases such as zeolites (phillipsite, natrolite, analcime) are also sporadically found. Based on petrography, chemical composition (Table 1 and supplementary Table 1, available in the online Supplementary materials at https://doi.org/xxxx), CIPW norm and classification diagrams (T.A.S.; Le Maitre *et al*. 1989, Fig. 4; R_1-R_2; De La Roche *et al*. 1980, not shown), the Ankililoaka volcanic rocks are basanites (ol > 10% in the CIPW norm, 6.2-16.9% normative nepheline) and alkali basalts.

Mineral chemistry. Representative analyses of the observed phases are reported in the supplementary Tables 2 to 9. Pressure, temperature and oxygen fugacity calculations were performed by using main minerals (i.e. olivine, clinopyroxene, and Fe-Ti oxides) and bulk-rock compositions.

Olivine composition in basanites ranges from Fo_{86} to Fo_{68} (Fo = molar Mg*100/(Mg+Fe)) from the cores through the rims to the rare groundmass microlites. Mantle olivine xenocrysts range from Fo_{88} to Fo_{90}. An increase in calcium and manganese and decrease in nickel is observed from cores to rims; no reverse zoning was observed. The alkali basalts have olivine Fo_{79-72} with slight normal zoning. Mantle olivine xenocrysts are present also in alkali basalts, with Fo_{92-90} composition (supplementary Table 2; Fig. 5*a*). The olivine-liquid equilibration temperatures (according to Roeder and Emslie, 1970) range from 1140 °C to 1217°C in the basanites, and from 1140 to 1170 °C in the alkali basalts.

Chromiferous, Al-rich **spinel** is found as inclusions in olivine crystals; Cr# (100*Cr/(Cr+Al) in atoms) ranges from 35 to 58 (supplementary Table 3).

Chromiferous, Al-rich spinel grades continuously to the Ti-magnetite of the groundmass (Fig. 5*b*). The wide compositional range observed in chromiferous, Al-rich spinel of basanites indicate independent mafic parental magmas.

The ubiquitous groundmass **Ti-magnetite** has ulvöspinel ranging from 30-67 mol.% in basanites and 17-73 mol.% in alkali basalts. The Al_2O_3 concentration in Ti-magnetite ranges from 1 to 8 wt.%, whereas MgO reaches values as high as 6.5 wt.%. **Ilmenite** is also present in alkali basalts; MnO concentration is ca. 1.5 wt.%, whereas vanadium is variable (V_2O_3 = 0.17-1.16 wt.%; supplementary Table 4). Magnetite/ ilmenite pairs in alkali basalts provide an equilibration temperature ranging from 768 °C to 939 °C, and an oxygen fugacity close to the NNO buffer.

Clinopyroxene in basanites and alkali basalts ranges from diopside (Mg# = 86) to titanaugite (Mg# = 69; supplementary Table 5; Fig. 5*c*; TiO_2 and Al_2O_3 up to 4.9 wt.% and 10 wt.%, respectively, roughly equivalent to 14 mol.% $CaTiAl_2O_6$ and 2 mol.% $CaFe^{3+}AlSiO_6$), with a negative correlation between Mg and Ti (and Al). With the exception of a few Mg-rich bulk compositions, the most Mg-rich olivine and clinopyroxene are in broad chemical (and textural) equilibrium with the host rocks. Clinopyroxene-liquid equilibrium temperatures (Putirka 2008) vary from 1015 to 1136 °C for basanites and 1064 to 1156 °C for alkali basalts. Pressure estimates for Mg-rich clinopyroxene phenocrysts range from 1 to 3 kbar (one pyroxene analysis giving 7 kbar), according to the clinopyroxene barometer of Nimis (1999), indicating their low-pressure origin by crystallization during the ascent in the crust.

Plagioclase in the basanites and alkali basalts is mostly labradorite and andesine (An_{35-68}), with very few bytownite (An_{74}; supplementary Table 6; Fig. 5*d*); some crystals have high SrO (up to 2.2 wt.%). The more Na-rich plagioclase of the groundmass is very often accompanied by hyalophane (An_{2-8} Ab_{24-30} Or_{45-60} Cn_{10} Sl_{5-6}; up to 5.4-5.6 wt.% BaO and 1.7-2.3 wt.% SrO, in groundmass crystals of samples M902 and M921) and abundant sanidine (up to Or_{80}). Anorthoclase compositions are rare.

The **nepheline** found in the groundmass of most basanites is Si-rich ($Q_4Ne_{85}Ks_{11}$ to $Q_{24}Ne_{70}Ks_6$, in wt.%), as usual in the nepheline of the other alkaline districts of Madagascar, and reaches an unusual, K-free composition, resembling a "jadeite"

($Q_{32}Ne_{68}Ks_0$; Na_2O = 14 wt.%; supplementary Table 7), in the groundmass of the alkali basalt M924. **Sodalite** is also frequently found (supplementary Table 7).

Apatite is F and Cl-bearing (up to 4.5 and 1.5 wt.% respectively; supplementary Table 8); sulphur is negligible, and REE_2O_3 are low (up to 1.36 wt.%). Very rare **Ba-phlogopite** (BaO = 4.9–7.0 wt.%; Table S9) and ferro-**kaersutite** (MgO=7-8.5 wt.%; TiO_2 = 6-9 wt.%; supplementary Table 9) occur sporadically in vugs. Secondary zeolites are frequent.

Xenoliths are represented by accidental quartz xenocrysts surrounded by clinopyroxene microliths, or vitrophyric lithics entrained in the Ambohitra neck. Augite and pigeonite xenocrysts were also found in the glassy lithics of the Ambohitra neck, indicating that an evolved tholeiitic magma could have been entrained in the host alkali basalt lava (Fig. 5*c*).

5. Geochemistry

The whole-rock major and trace element data for the Ankililoaka volcanic rocks are presented in Table 1 and supplementary Table 1. Most of the Ankililoaka samples have values of loss on ignition (L.O.I.) <2.5 wt.%, indicating that they are relatively fresh, consistently with petrographic observations. The basanites have MgO between 7.6 and 13.0 wt.%, and Mg# between 52 and 67 [Mg# = molar Mg*100/(Mg+Fe)]. TiO_2 content ranges from 2.2 to 3.6 wt.%. The Ni and Cr of the Mg-rich basanites (M919, M920, M921; Ni = 230-245 ppm; Cr = 480-520 ppm) are close or within the ranges expected for primary magmas. The concentration of Nb and Zr in the Mg-rich basanites range from 60 to 65 ppm and from 227 to 251 ppm, respectively. The more differentiated basanites are characterized by low to moderate concentration of Ni (84-128 ppm) and Cr (138-300 ppm) and high concentration of Nb (84-104 ppm) and Zr (334-471 ppm). The alkali basalts are characterized by moderate concentration of TiO_2 (2.1-2.4 wt.%), Nb (49–67 ppm) and Zr (204-241 ppm). MgO ranges from 6.7 to 9.3 wt.% (Mg# = 50-58). The Th/U ratio varies slightly (3.7-4.4) whereas the Nb/U ratio ranges from 30 to 39 in the more differentiated basanites, from 46 to 50 in the Mg-rich basanites and from 25 to 35 in the alkali basalts. The Ce/Pb varies from 20 to 36. The chondrite-normalized REE patterns (Fig. 6) do not show troughs at Eu, and the LREE/HREE ratios increase from alkali basalts (La_n/Yb_n = 19) to basanites (La_n/Yb_n = 30), the latter being generally less evolved. The alkali basalt M922 has La_n/Yb_n = 31. Basanites and alkali basalts have similar primitive mantle-normalized patterns (Fig. 7) with marked troughs at Rb, K and Pb, and peaks at Nb and Ta, as typical of within-plate mafic volcanic rocks of sodic affinity, and, in general, of the Cenozoic mafic magmatism throughout Madagascar (cf. Melluso *et al*. 2016).

6. $^{40}Ar/^{39}Ar$ ages

Three samples were selected for $^{40}Ar/^{39}Ar$ geochronology. The results are summarized in Table 2 and full analytical data are available in the supplementary Table 11. All three analyzed samples yielded robust plateau ages, defined by over 90% of the released gas (^{39}Ar). All samples show MSWD values between 0.12 and 1.07 and probability between 0.37 and 1.0. Analytical uncertainties (2σ) are small (< 0.12 Ma). Groundmass separated from the basanite sample M902 gave a plateau age of 12.03 ± 0.09 Ma (mean standard weighted deviation, MSWD = 0.12; probability, P = 1.0; Fig. 8*a*), including 97.5% of the total ^{39}Ar released. The inverse isochron age is concordant with the plateau age at 2σ and the initial $^{40}Ar/^{36}Ar$ ratios are atmospheric (297.2 ± 4.5). Groundmass separated from the basanite M914 yielded a plateau age of 10.55 ± 0.06 Ma (MSWD = 1.07; P = 0.37; Fig. 8*b*), including 100% of the ^{39}Ar released. The isochron age (10.87 ± 0.20 Ma) and the initial $^{40}Ar/^{36}Ar$ ratio (296.1 ± 1.5) are indistinguishable from the plateau age and air ratio, respectively. Groundmass separated from the basanite M918 also yielded a well-defined plateau age of 11.50 ± 0.11 Ma (MSWD = 0.25; P = 1.0; Fig. 8*c*), including 93.9% of the ^{39}Ar released, with an inverse isochron age of 11.35 ± 1.38 Ma (MSWD = 0.27) and $^{40}Ar/^{36}Ar$ initial value of 299.6 ± 10.5. All groundmass separates show decreasing K/Ca related to increase of degassing temperatures; this indicates that a high-Ca mineral phase, likely the groundmass plagioclase, was preferentially become degassed at higher temperatures.

The $^{40}Ar/^{39}Ar$ data constrain the beginning of the magmatism in the Ankililoaka area to about 12 Ma, significantly earlier than suggested by published K/Ar ages (9.37 ± 0.29 Ma and 8.95 ± 0.24 Ma; Bardintzeff *et al*. 2010).

7. Sr-Nd-Pb Isotopes

The Sr, Nd and Pb isotope compositions of the rocks of the Ankililoaka district are reported in Table 3 and Fig. 9. The basanites and alkali basalts have a limited range of initial (at 11 Ma) $^{87}Sr/^{86}Sr$ (0.70343 to 0.70383) and $^{143}Nd/^{144}Nd$ (0.512792 to 0.512822; ε_{Nd}=+3.1 to +3.6) and plot in the depleted field relative to Bulk Earth in the $^{143}Nd/^{144}Nd$ vs. $^{87}Sr/^{86}Sr$ diagram (Fig. 9*a*). Sample M914 has $^{87}Sr/^{86}Sr$ (0.70451) higher than the other basanites and alkali basalts. The basanite samples M904 and M905 of the aligned cones have the lowest $^{87}Sr/^{86}Sr$ (0.70343-0.703484) and the highest $^{143}Nd/^{144}Nd$ (0.512792-0.512822), whereas the alkali basalts have the highest $^{87}Sr/^{86}Sr$ (0.70373-0.70383). The Ankililoaka basanites and alkali basalts plot above the Northern Hemisphere Reference Line (NHRL) of Hart (1984), to the right of the 4.55 Ga geochron in the $^{207}Pb/^{204}Pb$ vs. $^{206}Pb/^{204}Pb$ diagram (Fig. 9*b*). The alkali basalts have lower $^{206}Pb/^{204}Pb$ (18.84-18.92) than the basanites (19.08-19.38) and also lower $^{208}Pb/^{204}Pb$ (<39 vs. >39) at roughly the same $^{207}Pb/^{204}Pb$. The Sr, Nd and Pb isotope compositions of Ankililoaka volcanic rocks can be considered as broadly representative of the mantle source of the magmas. The Ankililoaka rocks partially overlap with the volcanic mafic rocks of northern Madagascar (Fig. 9), although they have a different range of $^{87}Sr/^{86}Sr$ and $^{143}Nd/^{144}Nd$ and uniform $^{207}Pb/^{204}Pb$ (15.607-15.640). On the other hand, the isotope composition of Ankililoaka samples differs markedly from the mafic volcanic rocks of central Madagascar, which are generally characterized by lower $^{206}Pb/^{204}Pb$ and $^{207}Pb/^{204}Pb$ and higher $^{87}Sr/^{86}Sr$ (Fig. 9).

8. Discussion

The Ankililoaka district is a small monogenetic volcanic field (McGee & Smith 2016) formed by scattered emission centres, which are broadly aligned to NE-SW regional faults. The Ankililoaka basanites were erupted to the east of the Tulear fault, whereas the alkali basalts were emplaced to the west. The Tulear fault probably represents a boundary of lithospheric sectors having decreasing thickness towards the Mozambique Basin. It is unknown if this fault was active in the Late Miocene. More differentiated basanites were emplaced along the cone alignment (Androanzonkily to Betioky), whereas the more primitive rocks products form the almost flat cones at Ampasikibo. The similar $^{40}Ar/^{39}Ar$ ages of 10.6-12.1 Ma, 11.3 Ma and 8.6 Ma reported by Cucciniello *et al*. (2010, 2016, 2017) and Tucker *et al*. (2008) for volcanic rocks of Bobaomby, Massif d'Ambre, Ankaratra, Takarindiona and Lac Alaotra (Fig. 1*a*) indicate that the volcanism was synchronous within a Cenozoic (Mio-Pliocene) magmatic episode in Madagascar, and that the Ankililoaka volcanic field marks events of active extensional tectonics in the island. The rocks (basanites and alkali basalts) show a limited range of magmatic evolution, as expected by mafic magmas excaped from ponding in shallow magma reservoirs, and do not indicate liquid lines of descent to evolved compositions.

The Ankililoaka basanites and alkali basalts have low Zr/Nb (3.6-4.9), Ba/Nb (8.6-28.4) and high Zr/Y (5.3-11.7) and La/Yb (28-46). The ratios between incompatible elements match those of Massif d'Ambre, Bobaomby, Ampasindava, Nosy Be, Ankaratra, Itasy, Alaotra and Takarindiona mafic rocks (Massif d'Ambre: Zr/Nb = 2.4-5.8 and Ba/Nb = 6.7-23.9; Bobaomby: Zr/Nb = 2.5-4.1 and Ba/Nb = 9.8-16.3; Ampasindava: Zr/Nb = 3.0-5.7 and Ba/Nb = 7.4–15.9; Nosy Be: Zr/Nb = 2.7-4.4 and Ba/Nb = 7.7-15.2; Ankaratra: Zr/Nb = 2.1-5.2 and Ba/Nb = 8.6-13.7; Itasy: Zr/Nb = 3.8-4.3 and Ba/Nb = 8.3-11.6; Alaotra: Zr/Nb = 2.8-3.4 and Ba/Nb = 7.3-12.8; Takarindiona: Zr/Nb = 2.2-3.7 and Ba/Nb = 8.2-12.4; data from Melluso & Morra 2000; Melluso *et al*. 2007, 2011, 2016; Cucciniello *et al*. 2011, 2016). The patterns of Ankililoaka basanites and alkali basalts (in primitive mantle-normalized incompatible element diagram, Fig. 7) are similar to those of other Madagascar Cenozoic mafic rocks. Nevertheless, the more differentiated basanites of Ankililioaka show higher absolute concentrations of LREE and HFSE than the other Ankililoaka and Cenozoic Madagascar mafic rocks. The systematic differences in the major and trace elements of Ankililoaka samples (supplementary Fig. 2) can be attributed to source heterogeneity (or different mantle source), rather than to the effect of differentiation processes. The highly alkaline nature of the Ankililoaka volcanic rocks is testified by the intrasample variations of mineral chemistry and mineral assemblages, from the olivine phenocrysts to the late-crystallized feldspathoids. Basanites and alkali basalts are by far the most common rock types in the Cenozoic volcanism of Madagascar (e.g. Melluso *et al*. 2016 and references therein).

Crustal contamination

Significant upper crustal contamination of the Ankililoaka mafic rocks is considered unlikely on the basis of the following arguments: 1) upper crustal contamination would lead to a modification of key trace element ratios (especially LILE/HFSE ratios) that, on the other hand, remain roughly uniform (and low) in the Ankililoaka mafic rocks; 2) the peaks at Nb and troughs at Pb in the mantle-normalized diagrams; 3) the values of Sr-Nd-Pb isotope ratios of Ankililoaka volcanic rocks are typical of mantle-derived melts.

Temperature and pressure estimates of melting

The presence of mantle olivine xenocrysts in some basanites and alkali basalts indicates a short residence time of the magma in the continental crust. This makes the Ankililoaka mafic rocks potential tools to infer the chemical composition of their mantle sources. However, to allow evaluation of partial melting processes and source region characteristics of Ankililoaka rocks, it is necessary to consider only compositions representative of magmatic liquids. On the basis of petrography, the Ankililoaka lavas can be considered to be liquid compositions. These lavas have between 6.7 and 12.7 wt.% MgO (Mg# = 50-67) and are generally mildly porphyritic. The samples with highest Mg# are not too far from primary magma and appear to be saturated only in olivine. To determine a possible primary magma composition for the Ankililoaka lavas, we have used the Excel programme of Lee *et al*. (2009). This calculation requires that the magma composition used is saturated only in olivine, and adds back equilibrium olivine until a magma composition is obtained that is in chemical equilibrium with mantle peridotite. Only the samples with MgO > 9 wt.% were considered. The results of the parental melt calculations are summarized in supplementary Table 11. The model of Lee *et al*. (2009) suggests that ~15% olivine needed to be added to reach the equilibrium composition.

The calculated temperatures range from 1444 to 1529°C (these temperatures are heavily over-estimated if the source region of Ankililoaka magmas is more fertile than ambient mantle, or hydrous), with pressures of melting between 2.3 and 3.1 GPa for alkali basalts and between 3.0 and 3.8 GPa for basanites. If these results are considered reliable (considering also that the database of Lee *et al*. 2009 was only on anhydrous and not-alkaline rocks), they indicate a mantle source at 80-95 km, close to the garnet–spinel peridotite transition (2.8-3.1 GPa; Robinson &Wood 1998). On the basis of the shear-velocity model proposed by Pratt *et al*. (2017), a low-shear velocity anomaly is identified at depths 50-150 km beneath the Ankililoaka area (Fig. 10). This low-velocity anomaly could be linked to upwelling mantle, as well as to the presence of melts or light phases such as amphiboles.

Mantle source characteristics of the Ankililoaka magmatism

The enriched geochemical characteristics of Ankililoaka mafic rocks are evident from the low Zr/Nb (< 5), La/Nb (0.8-1.4), Lu/Hf (0.039-0.067) and high Zr/Y (8-14) ratios, typical of oceanic alkali basalts (OIB) and intraplate continental alkaline rocks. Incompatible trace element and isotope ratios show small differences between the different plugs, scoria cones and lava flows of Ankililoaka district (Tables 1, 3 and supplementary Table 1; Fig. 6, 7, 9), implying some heterogeneity in their respective source regions.

A useful approach to model partial melting of mantle sources is based on variation of REE concentration and ratios (e.g. the variation of La/Yb vs. Gd/Yb; of Fig. 11). Such variations can help distinguish between melting in the garnet peridotite stability field and melting in the spinel peridotite stability field because of the strong fractionation of HREE by residual garnet, as noted elsewhere in the Cenozoic magmatism of Madagascar (cf. Melluso *et al*. 2011, 2016). The approach

can be considered only semi-quantitative because several assumptions (e.g. the composition of the source, the abundance of minerals in the starting assemblage, the type of partial melting, the assumed partition coefficients and so on) have been chosen *ad hoc* (supplementary Table 13) and cannot be rigorously verified.
The range of compositions of calculated melts (assuming low degrees of melting ranging from 1 to 5%) from spinel- and garnet- bearing peridotitic sources, starting from a incompatible element-enriched mantle (up to three times primitive mantle for the most incompatible elements and primitive mantle for heavy rare earth elements) indicates that the Ankililoaka lavas could derive from mixing of melts formed at different depths (Fig. 11).

Pyroxenites may have contributed to the source of the Ankililoaka rocks. Herzberg & Asimow (2008) suggested that the relationship of MgO and CaO could be used as a potential indicator of pyroxenitic sources. Magmas from pyroxenite sources should generally exhibit lower CaO at a given MgO compared to magmas from peridotite sources. In the CaO vs. MgO diagram, the Ankililoaka primary melts plot in the field of melts from peridotite (Fig. 12). Only the basaltic compositions plot on the hypothetical line that divide peridotite- from pyroxenite-derived melts. Finally, using the source indicator FC3MS (FeO/CaO-3*MgO/SiO_2, all in wt.%) of Yang & Zhou (2013; a parameterization of melting experiments on a variety of peridotite and pyroxenite sources), the Ankililoaka rocks plot in the field of melts from peridotite mantle.

The primitive mantle normalized patterns (Fig. 7) indicate that Ankililoaka rocks are depleted in K relative to Nb, Th or La, elements of similar degree of incompatibility. The trough at potassium can be explained by a potassium-depleted source mantle or by the presence of residual potassium-bearing phases in the source during the melting, such as amphibole or phlogopite. Melluso & Morra (2000), Cucciniello *et al*. (2011, 2016) and Melluso *et al*. (2007*b*, 2011, 2016) propose that the trough at K in the patterns of Cenozoic Madagascar olivine melilitites, olivine nephelinites, basanites, alkali and tholeiitic basalts as broadly inherited from the mantle source. Amphibole is indeed present in the mantle beneath Madagascar (e.g. Rocco *et al*. 2017), but it is unlikely to be a residual phase during melting. The concentration of K of the Ankililoaka rocks is also too low (on the order of ~30-70 times primitive mantle) to be in equilibrium with residual phlogopite (e.g. Späth *et al*. 2001). The available petrogenetic studies indicate that the Cenozoic mafic rocks of central and northern Madagascar were derived from variably incompatible element-enriched lithospheric mantle at different depths (from garnet-bearing to spinel-bearing mantle; Melluso *et al*. 2016 and references therein).

9. Conclusions

The sporadic Cenozoic volcanic rocks in southwestern Madagascar are sodic alkaline to strongly alkaline, and emplaced along the regional NNW-SSE fault system, already well known in the Morondava basin. The $^{40}Ar/^{39}Ar$ ages of 10.6-12 Ma match those of other volcanic rocks in central and northernmost Madagascar and help to better constrain an extensional event that took place throughout the island. The Ankililoaka rocks have limited compositional range, and their geochemical and isotopic characteristics are more similar to those of the mafic rocks cropping out in the northernmost Madagascar, rather than the alkaline volcanic rocks in the central and northeast Madagascar. The geochemical characteristics of basanites and alkali basalts of the Ankililoaka district indicate derivation by low-degree partial melting of a highly enriched peridotitic mantle lithosphere, placed beneath the Proterozoic mobile belts surrounding the cratonized core of Madagascar. The melting event is interpreted to have been triggered by the extensional events that caused uplift of the central Madagascar backbone in the Cenozoic, and have no relationship to the Gondwana breakup, nor with the opening or movements in the Mozambique Basin, located just to the east.

Acknowledgements

Vincenzo Monetti helped in sampling, A. Langella, R. de' Gennaro, P. Le Roux and S. Bravi kindly helped in the field and in the laboratory work. Advice from Christian Nicollet was deeply appreciated. The field trip of 2014 was granted by

MIUR (grants 2010-2011) and the analytical work was granted by MIUR 2015 (to L.M.) and Fondi Ricerca di Ateneo (DR_3450_2016 to C.C.).

References

Bardintzeff, J.-M., Liegeois, J.-P., Bonin, B., Bellon, H. & Rasamimanana, G. 2010. Madagascar volcanic provinces linked to the Gondwana break-up: geochemical and isotopic evidences for contrasting mantle sources. *Gondwana Research* **18**, 295-314.

Battistini, R. 1962. Le massif volcanique de l'Itasy (Madagascar). *Annales de Geographie* **384**, 167-178.

Besairie, H. 1964. *Geological map of Madagascar*. Service Geologique de Madagascar, Tananarive.

Boynton, W. V. 1984. Cosmochemistry of the rare earth elements: meteorite studies. *In*: Henderson P., (ed) *Rare Earth Element Geochemistry*. Elsevier, Amsterdam, 63–114.

Cucciniello, C., Langone, A., Melluso, L., Morra, V., Mahoney, J. J., Meisel, T. & Tiepolo, M. 2010 U-Pb ages, Pb-Os isotope ratios, and platinum-group element (PGE) composition of the West-Central Madagascar flood basalt province. *Journal of Geology* **118**, 523–541. http://dx.doi.org/10.1086/655012.

Cucciniello, C., Tucker, R. D., Jourdan, F., Melluso, L. & Morra, V. 2016. The age and petrogenesis of the alkaline magmatism of Ampasindava Peninsula and Nosy Be archipelago, northern Madagascar. *Mineralogy and Petrology* **110**, 309–331. http://dx.doi.org/10.1007/s00710-015-0387-1.

Cucciniello, C., Melluso, L., le Roex, A. P., Jourdan, F., Morra, V., de' Gennaro, R. & Grifa, C. 2017. From nephelinite, basanite and basalt to peralkaline trachyphonolite and comendite in the Ankaratra volcanic complex, Madagascar: $^{39}Ar/^{40}Ar$ ages, phase compositions and bulk-rock geochemical and isotopic evolution. *Lithos* **274-275**, 363-382. http://dx.doi.org/10.1016/j.lithos.2016.12.026.

Cucciniello, C., Melluso, L., Morra, V., Storey, M., Rocco, I., Franciosi, L., Grifa, C., Petrone, C. M. & Vincent, M. 2011. New ^{40}Ar-^{39}Ar ages and petrogenesis of the Massif d'Ambre volcano, northern Madagascar. *In*: Beccaluva L., Bianchini G. & Wilson M. (eds) *Volcanism and Evolution of the African Lithosphere*. Geological Society of America Special Papers **478**, 257-282. http://dx.doi.org/10.1130/2011.2478(14).

De La Roche, H., Leterrier, P., Grandclaude, P., Marchal & E. 1980. A classification of volcanic and plutonic rocks using R_1-R_2 diagram and major element analyses. Its relationships with current nomenclature. *Chemical Geology* **29**, 183-210.

de Wit, M. J., Bowring, S. A., Ashwal, L.D., Randrianasolo, L. G., Morel, V. P. I. & Rambeloson, R. A. 2001. Age and tectonic evolution of Neoproterozoic ductile shear zones in southwestern Madagascar, with implications for Gondwana studies. *Tectonics* **20**, 1-45. 2000TC900026.

Estrade, G., Béziat, D., Salvi, S., Tiepolo, M., Paquette, J.-L. & Rakotovao, S. 2014. Unusual evolution of silica-under- and -oversaturated alkaline rocks in the Cenozoic Ambohimirahavavy Complex (Madagascar): mineralogical and geochemical evidence. *Lithos* **206-207**, 361–383.

Galer, S. J. G. & Abouchami, W. 1998. Practical application of lead triple spiking for correction of instrumental mass discrimination. *Mineralogical Magazine* **62A**, 491–492.

Hart, S. R. 1984. A large-scale anomaly in the Southern Hemisphere mantle. *Nature* **309**, 753–757.

Herzberg, C. & Asimow, P. D. 2008. Petrology of some oceanic island basalts: PRIMELTS.XLS software for primary magma calculation. *Geochemistry Geophysics Geosystems* **9**, Q09001.

Jöhns, N. & Schenk, V. 2008. Relics of the Mozambique Ocean in the central East African Orogen: evidence from the Vohibory Block of southern Madagascar. *Journal of Metamorphic Geology* **26**, 17-28 http://dx.doi.org/10.1111/j.1525-1314.2007.00745.

Koppers, A. A. P. 2002. ArArCALC–software for $^{40}Ar/^{39}Ar$ age calculations. *Computers & Geosciences* **28**, 605-619.

Lacroix ,A. 1922–1923. *Mineralogie de Madagascar*. Augustin Challamel, Paris, vol. 1–3.

Lee, C.-T. A., Luffi, P., Plank, T., Dalton, H. & Leeman, W. P. 2009. Constraints on the depths and temperatures of basaltic magma generation on Earth and other terrestrial planets using new thermobarometers for mafic magmas. *Earth and Planetary Science Letters* **279**, 20-33.

Lee, J.-Y., Marti, K., Severinghaus, J. P., Kawamura, K., Yoo, H.-S., Lee, J. B. & Kim, J. S. 2016. A redermination of the isotopic abundances of atmospheric Ar. *Geochimica et Cosmochimica Acta* **70**, 4507-4512.

Le Maitre, R. W., Bateman, P., Dudek, A., Keller, J., Lameyre, J., Le Bas, M. J., Sabine, P. A., Schmid, R., Sorensen, H., Streckeisen, A., Woolley, A. R. & Zanettin, B. 1989. *A Classification of Igneous Rocks and Glossary of Terms: Recommendations of the International Union of Geological Sciences, Subcommission on the Systematics of Igneous Rocks*. Blackwell Scientific, Oxford 193 pp.

le Roex, A. P., Chevallier, L., Verwoerd, W. J. & Barends, R. 2012. Petrology and geochemistry of Marion and Prince Edward islands, Southern Ocean: magma chamber processes and source region characteristics. *Journal of Volcanology and Geothermal Research* **223-224**, 11-28.

Lyubetskaya, T. & Korenaga, J. 2007. Chemical composition of Earth's primitive mantle and its variance: 1. methods and results. *Journal of Geophysical Research* **112**, B03211 doi: 10.1019/2005JB004223.

McGee, L. E. & Smith, I. E. M. 2016. Interpreting chemical compositions of small scale basaltic systems: a review. *Journal of Volcanology and Geothermal Research* **325**, 45-60.

Mahoney J. J., le Roex A. P., Peng Z. X., Fisher R. L. & Natland J. H. 1992. Southwestern limit of Indian Ocean ridge mantle and the origin of low $^{206}Pb/^{204}Pb$ MORB: isotope systematics of the central southwest Indian Ridge (17°–50°E). *Journal of Geophysical Research* **97**, 19,771–19,790.

Melluso, L., Guarino, V., Lustrino, M., Morra, V. & de' Gennaro, R. 2017. The REE- and HFSE-bearing phases in the Itatiaia alkaline complex (Brazil) and geochemical evolution of feldspar-rich felsic melts. *Mineralogical Magazine* **81**, 217-250. https://doi.org/10.1180/minmag.2016.080.122.

Melluso, L., Cucciniello, C., le Roex, A. P. & Morra, V. 2016. The geochemistry of primitive volcanic rocks of the Ankaratra volcanic complex, and source enrichment processes in the genesis of the Cenozoic magmatism in Madagascar. *Geochimica et Cosmochimica Acta* **185**, 435-452. http://dx.doi.org/10.1016/j.gca.2016.04.005

Melluso, L., le Roex, A.P. & Morra, V. 2011 Petrogenesis and Nd-Pb-Sr- isotope geochemistry of the olivine melilitites and olivine nephelinites ("ankaratrites") in Madagascar. *Lithos* **127**, 505-521. http://dx.doi.org/10.1016/j.lithos.2011.08.003.

Melluso, L. & Morra, V. 2000. Petrogenesis of late Cenozoic mafic alkaline rocks of the Nosy Be archipelago (northern Madagascar): relationships with the Comorean magmatism. *Journal of Volcanology and Geothermal Research* **56**, 129-142.

Melluso, L., Morra, V., Brotzu, P., Franciosi, L., Grifa, C., Lustrino, M., Morbidelli, P., Riziky, H. & Vincent, M. 2007*a*. The Cenozoic alkaline magmatism in central–northern Madagascar: a brief overview. *Periodico di Mineralogia* **76**, 169-180.

Melluso, L., Morra, V., Riziky, H., Veloson, J., Lustrino, M., Del Gatto, L. & Modeste, V. 2007*b*. Petrogenesis of a basanite-tephrite-phonolite volcanic suite in the Bobaomby (Cap d'Ambre) peninsula, northern Madagascar. *Journal of African Earth Sciences* **49**, 29-42.

Melluso, L., Morra, V., Guarino, V., de' Gennaro, R., Franciosi, L. & Grifa, C. 2014. The crystallization of shoshonitic to peralkaline trachyphonolitic magmas in a HO–Cl–F-rich environment at Ischia (Italy), with implications for the feeder system of the Campania Plain volcanoes, *Lithos* **210**, 242-259. http://dx.doi.org/10.1016/j.lithos.2014.10.002.

Nicollet, C. 1984. Le volcanism dans le Sud-Ouest de Madagascar. *Journal of African Earth Sciences* **2**, 383-388.

Nimis, P. 1999. Clinopyroxene geobarometry of magmatic rocks. Part 2. Structural geobarometers for basic to acid, tholeiitic and mildly alkaline magmatic systems. *Contributions to Mineralogy and Petrology* **135**, 62-74.

Phethean, J. J. J., Kalnins, L. M., van Hunen, J., Biffi, P. G., Davies, R. J. & McCaffrey, K. J. W. 2017. Madagascar's escape from Africa: A high-resolution plate reconstruction for the Western Somali Basin and implications for supercontinent dispersal. *Geochemistry Geophysics Geosystems* **17**, 5036-5055, http://dx.doi.org/10.1002/2016GC006624.

Phillips, D. & Matchan, E. L. 2013. Ultra-high precision Ar/Ar ages for Fish Canyon Tuff and Alder Creek Rhyolite sanidine: New dating standards required? *Geochimica et Cosmochimica Acta* **121**, 229-239. http://dx.doi.org/10.1016/j.gca.2013.07.003.

Piqué, A., Laville, E., Chotin, P., Chorovicz, J., Rakotondraompiana, S. & Thouin, C. 1999. L'extension a Madagascar du Neogene a l'Actuel: arguments structuraux et geophysiques. *Journal of African Earth Sciences* **28**, 975-983.

Pratt, M. J., Wysession, M. E., Aleqabi, G., Wiens, D. A., Nyblade, A. A., Shore, P., Rambolamanana, G., Andriampenomanana, F., Rakotondraibe, T., Tucker, R. D., Barruol, G. & Rindraharisaona, E. 2017. Shear velocity structure of the crust and upper mantle of Madagascar derived from surface wave tomography. *Earth and Planetary Science Letters* **458**, 405-417. https://doi.org/10.1016/j.epsl.2016.10.041.

Putirka, K. D. 2008. Thermometers and barometers for volcanic systems. *Reviews in Mineralogy and Geochemistry* **69**, 61-120.

Renne, P. R., Mundil, R., Balco, G., Min, K. & Ludwig, K. R. 2010. Joint determination of ^{40}K decay constants and ^{40}Ar*/^{40}K for the Fish Canyon sanidine standard, and improved accuracy for ^{40}Ar/^{39}Ar geochronology. *Geochimica et Cosmochimica Acta* **74**, 5349-5367.

Rindraharisaona, E. J., Tilmann, F., Yuan, X., Rümpker, G., Giese, J., Rambolamanana, G. & Barruol, G. 2017. Crustal structure of southern Madagascar from receiver functions and ambient noise correlation:

Implications for crustal evolution. *Journal of Geophysical Research* **122**, 1179-1197. 10.1002/2016JB13565

Robinson, J. A. C. & Wood, B. J. 1998. The depth of the spinel to garnet transition at the peridotite solidus. *Earth and Planetary Science Letters* **164**, 277-284.

Rocco, I., Zanetti, A., Melluso, L. & Morra, V. 2017. Ancient depleted and enriched mantle lithosphere domains in northern Madagascar: geochemical and isotopic evidence from spinel-to-plagioclase-bearing ultramafic xenoliths. *Chemical Geology* **466**, 70-85. http://dx.doi.org/10.1016/j.chemgeo.2017.05.016

Roeder, P. L. & Emslie, R. F. 1970. Olivine-liquid equilibrium. *Contributions to Mineralogy and Petrology* **29**, 275-289.

Späth, A., le Roex, A. P., Opiyo-Akech, N., 2001. Plume-lithosphere interaction and the origin of continental rift-related alkaline volcanism – the Chyulu Hills volcanic province, southern Kenya. *Journal of Petrology* **42**, 767-787.

Storey, M., Mahoney, J. J., Saunders, A. D., Duncan, R. A., Kelley, S. P. & Coffin, M. F. 1995. Timing of hot spot-related vulcanism and the breakup of Madagascar and India. *Science* **267**, 852-855.

Tucker, R. D., Conrad, J., Key, R. M., Pitfield, P. E. J., Randriamananjara, T., Taylor, C. D., Goodenough, K. M. & Thomas, R. J. 2008. *$^{40}Ar/^{39}Ar$ geochronology of Mesozoic and younger igneous rocks, Madagascar*, in "Revision of the geologic and mineral cartography of the north, central and east- central zones of Madagascar"; explanatory note to the Republic of Madagascar, Ministry of Energy and Mines (MEM/SG/DG/UCP/ PGRM); Geologic and Commission Report - British Geological Survey, Report: **CR/08/078**, 385–435, 1 Appendix.

Tucker, R. D., Roig, Y. G., Moine, B., Delor, C. & Peters, S. G. 2014. A geological synthesis of the Precambrian shield in Madagascar. *Journal of African Earth Sciences* **94**, 9-30.

Weis, D., Kieffer, B., Maerschalk, C., Barling, J., de Jong, J., Williams, G. A., Hanano, D., Pretorius, W., Mattielli, N., Scoates, J. S., Goolaerts, A., Friedman, R. M. & Mahoney, J. B. 2006. High-precision isotopic characterization of USGS

BHVO-1 and BHVO-2 reference materials by TIMS and MC-ICP-MS. *Geochemistry Geophysics Geosystems* 7, Q08006, http://dx.doi.org/10.1029/2006GC001283.

Yang, Z. F. & Zhou, J. H. 2013. Can we identify source lithology of basalt? *Scientific Report* **3**, 1856. http://dx.doi.org/10.1038/srep01856.

Appendix 1. Analytical techniques

The samples of this study were collected during a field trip in September 2014. Powders of the samples were obtained after carefully grinding washed chips in an ultrapure agate mill. Four grams of rock powder (for each samples) were used to prepare pressed powder pellets. The powder (mixed with 1 ml of Polyvinyl alcohol solution) was pressed to twenty tons for twenty seconds. The bulk-rock compositional data (supplementary Table 1) were determined on pressed powder pellets with an Axios Panalytical X-ray fluorescence (XRF) spectrometer equipped with six analyzer crystals, three primary collimators and two detectors (flow counter and scintillator), operating at different kV and mA for each analyte. Analytical uncertainties are in the order of 1-2% for major elements and 5-10% for trace elements.

Data on a subset of samples were obtained through ICP-MS methods at Actlabs (Canada) (Table 1). Samples are mixed with a flux of lithium metaborate and lithium tetraborate and fused in an induction furnace. The molten melt is immediately poured into a solution of 5% nitric acid containing an internal standard, and mixed continuously until completely dissolved (~30 minutes). The samples are run for major oxides and selected trace elements (Ba, Be, Sc, Sr, V, Y and Zr) on a combination simultaneous/sequential Thermo Jarrell-Ash ENVIRO II ICP or a Varian Vista 735 ICP. Calibration is performed using 7 prepared USGS and CANMET certified reference materials. One of the 7 standards is used during the analysis for every group of ten samples. Sample fused are diluted and analyzed by Perkin Elmer Sciex ELAN 6000, 6100 or 9000 ICP/MS for other trace elements (Cr, Co, Ni, Cu, Zn, Ga, Ge, As, Rb, Nb, Mo, Ag, In, Sn, Sb, Cs, La, Ce, Pr, Nd, Sm, Eu, Gd, Tb, Dy, Ho, Er, Tm, Yb, Lu, Hf, Ta, W, Tl, Pb, Bi, Th and U). Three blanks and five controls (three before the sample group and two after) are analyzed per group of samples. Duplicates are fused and analyzed every 15 samples. Analyses of international standards are reported in the supplementary Table 14.

The weight loss on ignition has been obtained with gravimetric techniques, firing at 1000°C small aliquots of powders previously dried at 110°C overnight.

$^{40}Ar/^{39}Ar$ dating was carried out on approximately 200 mg of groundmass material (150-250 µm grain size) hand-picked under a binocular microscope. Grains were leached in dilute HF for five minutes and then thoroughly rinsed with distilled water in an ultrasonic bath. The samples were then loaded in two separated discs (along with unrelated samples) into an aluminium foil packet, placed in a quartz tube, with the flux monitor standard Fish Canyon sanidine (FCs; 28.294 ± 0.036 Ma, 1σ; Renne *et al*. 2010) and irradiated for 3 hours in the Oregon State university nuclear reactor (USA) in central position. The discs were Cd-shielded (to minimize undesirable nuclear interference reactions) and irradiated in the Oregon State University nuclear reactor (USA) in central position. The mean J-values computed from standard grains within the small pits yielded values of 0.000854 (± 0.10%) and 0.0111724 (± 0.035%). Mass discrimination was monitored regularly through the analysis using an automated air pipette and provided mean values of 0.99571 (± 0.02%) and 0.99493 (± 0.03%) per dalton (atomic mass unit) relative to an air ratio of 298.56 ± 0.31 (Lee *et al*. 2016). The correction factors for interfering isotopes were $(^{39}Ar/^{37}Ar)_{Ca} = 7.6 \times 10^{-4}$ (± 1.2%), $(^{36}Ar/^{37}Ar)_{Ca} = 2.7 \times 10^{-4}$ (± 0.7%) and $(^{40}Ar/^{39}Ar)_{K} = 7.3 \times 10^{-4}$ (± 10%). The $^{40}Ar/^{39}Ar$ analyses were performed at the Western Australian Argon Isotope Facility at Curtin University. Groundmass populations (5 mg each) were step-heated using a continuous 100 W PhotonMachine© CO_2 (IR, 10.4 μm) laser fired on the grains during 60 seconds. Each of the standard crystals was fused in a single step.

The gas was purified in an extra low-volume stainless steel extraction line of 240cc and using one SAES AP10 and one GP50 getter. Ar isotopes were measured in static mode using a low volume (600 cc) ARGUS VI mass spectrometer from Thermofisher© (Phillips & Matchan 2013) set with a permanent resolution of ~200. Measurements were carried out in multi-collection mode using four faradays to measure mass 40 to 37 and a 0-background compact discrete dynode ion counter to measure mass 36. We measured the relative abundance of each mass simultaneously using 10 cycles of peak-hopping and 33 seconds of integration time for each mass. Detectors were calibrated to each other electronically and using Air shot beam signals. The raw data were processed using the ArArCALC software (Koppers 2002) and the ages have been calculated using the decay constants recommended by Renne *et al*. (2010). Blanks were monitored every 3 to 4 steps. All parameters and relative abundance values are reported in the supplementary Table 11 and have been corrected for blank, mass discrimination and radioactive decay. Individual errors in supplementary Table 11 are given at the 1σ level. The criteria for the determination of plateau are as follows: plateaus must include at least 70% of ^{39}Ar. The plateau should be distributed over a minimum of 3 consecutive steps agreeing at 95% confidence level and satisfying a probability of fit (P) of at least 0.05. Plateau ages are given at the 2σ level and are calculated using the mean of all the plateau steps, each weighted by the inverse variance of their individual analytical error. Uncertainty includes analytical and J-value errors. Errors with all sources of uncertainty are indicated by a square bracket (e.g., [±0.16 Ma]).

The Sr-Nd-Pb-isotope data were obtained at the University of Cape Town, with techniques described in le Roex *et al*. (2012). Sr, Nd and Pb were separated using conventional ion exchange techniques and all radiogenic isotope analyses were performed on a NuPlasma multicollector inductively coupled plasma-mass spectrometer (ICP-MS). To correct for mass fractionation effects, measured $^{87}Sr/^{86}Sr$ and $^{143}Nd/^{144}Nd$ values were normalized to $^{86}Sr/^{88}Sr = 0.1194$ and $^{146}Nd/^{144}Nd = 0.7219$, respectively. Pb isotopes were corrected for fractionation by normalizing ratios measured in international standards. Average standard values obtained during the course of this study are reported in the Table 3. Microprobe analyses were carried out on polished thin sections using Energy Dispersive Spectrometry (EDS) at University of Napoli Federico II, utilizing a JEOL JSM-5310 microscope operating at 15 kV primary beam voltage, 50-100 mA filament current, 40-50 s net acquisition time and a Oxford Instruments Microanalysis Unit, equipped with an INCA X-act detector. The analytical details are fully reported in Melluso *et al*. (2014, 2017)

Table Captions

Table 1: Representative bulk-rock analyses of the Ankililoaka samples. Major and minor element oxide values are in wt.%; trace element data are in ppm. L.O.I. (weight loss on ignition) was measured gravimetrically. bsn, basanite; alk bas, alkali basalt.

Table 2: Summary of $^{40}Ar/^{39}Ar$ results for the Ankililoaka samples. MSWD is mean square weighted deviate and p is the corresponding probability for plateau. Errors are reported at the 2σ confidence level.

Table 3: Sr-Nd-Pb isotopic compositions for the Ankililoaka samples. Subscripts "i" on Sr and Nd isotopic ratios indicate initial values (age-corrected to 11 Ma for Ankililoaka basanites and alkali basalts).

Figure captions

Figure 1: (a) Simplified geological map of Madagascar, showing the outcrops of Late Cretaceous (black and dark grey areas) and Cenozoic (light grey areas) igneous rocks. $^{40}Ar/^{39}Ar$ and U–Pb ages for the Madagascar Cenozoic igneous rocks (Cucciniello et al. 2016 and references therein) are also indicated. Simplified basement geology of Madagascar is also shown (after Tucker et al. 2014). (b) Sketch map of southwestern Madagascar (after Besairie 1964)

Figure 2: Sketch map of the Ankililoaka district, modified after the Geological Map of Madagascar (sheets Manombo-Manera 562-563) with the location of studied samples (gps coordinates in Table 1 and Supplementary Table 1).

Figure 3: Volcanologic features of the outcrops: a) the four aligned spatter cones of Betioky Nord as seen from the southern-most cone: the likely dyke feeding the cones is not visible at the present erosion level; b) breadcrust bombs on the

northern-most cone; c) the remnant of the neck west of Ampasikibo, the most magnesian basanite of the area: one of the aligned cones can be seen in the background; d) the Ampihamy lava field as seen from north; dykes can be seen in the foreground; e) the Ambohitra neck at the entrance of the Mikea National Park as seen from the NE; f) a spindle-shaped bomb at Ambohitra; g) columnar joints in a pit quarried in one of the two Androhazonily necks.

Figure 4: Total alkali-silica (T.A.S.) classification diagram for Ankililoaka volcanic rocks. Data of the Cenozoic mafic rocks (Cucciniello *et al*. 2017; Melluso *et al*. 2016 and references therein; small grey circles) are shown for comparison

Figure 5: Mineral compositions in the Ankililoaka samples. (a) whole-rock Mg# versus Fo content of olivines. The lines represent the Fe–Mg partition coefficient between olivine and liquid (K_d) = 0.30 ± 0.03 (Roeder & Emslie 1970). (b) Chromium-rich spinels. The spinels of other Cenozoic mafic lavas of Madagascar are also shown. (c) Pyroxene compositions projected in the Ca-Mg-Fe diagram. Also shown for comparison are compositional fields for pyroxenes in the Cenozoic mafic lavas of Madagascar (Cuccinello *et al*. 2017, 2016, 2011). (d) Feldspar compositions.

Figure 6: (a-b) Chondrite-normalized REE diagram for Ankililoaka samples. The chondrite values used for normalization are those of Boynton (1984). Prometium is interpolated.

Figure 7: (a-b) Primitive mantle-normalized incompatible element diagrams for Ankililoaka mafic rocks. Primitive mantle values are from Lyubetskaya & Korenaga (2007). Fields of the Cenozoic mafic rocks (Cucciniello *et al*. 2017, 2016, 2011; Melluso & Morra, 2000; Melluso et al., 2016, 2007) are shown for comparison.

Figure 8: Groundmass age spectra plots for the Ankililoaka basanites. The horizontal lines close to the plateau age indicate the steps used in the age calculation. Errors on plateau ages (plateaus include > 70 % ^{39}Ar released) are quoted at 2σ and include all sources of uncertainties. MSWD and P values are indicated.

Figure 9: (a-d) Sr-Nd-Pb isotopic compositions of Ankililoaka volcanic rocks. The Northern Hemisphere Reference Line (NHRL) and the geochron at 4.55 Ga are shown in the $^{206}Pb/^{204}Pb$ vs. $^{207}Pb/^{204}Pb$ isotope diagram. Data for the Cenozoic Madagascar igneous rocks are from Cucciniello *et al*. (2011), Melluso & Morra (2000), Melluso *et al*. (2016). Indian mid-ocean ridge basalt (MORB) data are from Mahoney *et al*. (1992).

Figure 10: Schematic cross-section of southern Madagascar through the shear-velocity model with respect to PREM (Preliminary Reference Earth Model) to 200 km depth (after Pratt *et al*. 2017). an upper-mantle low-velocity region, that is observable at 50 km depth, lies under the Ankililoaka area, but becomes much weaker with greater depth.

Figure 11: La/Yb vs. Gd/Yb diagram for the Ankililoaka mafic rocks and non-modal fractional melting modeling of a lherzolitic mantle source. The mode of the source is ol = 58-53%, cpx = 14-27%, opx = 26-16%, sp = 3% or gt = 4%. The amounts of minerals participating to the melt used in the model are: ol = -6-8%, cpx = 67-71%, opx = -19-28%, and sp/grt = 11-40%. Partition coefficients used in the model are from Melluso *et al*. (2016) and references therein. Formula used for non-modal fractional melting model: $C_l/C_0 = (1/f)*(1-(1-Pf/D)^{(1/P)})$, where C_l is the concentration of element in the liquid, C_0 the concentration of the element in the starting assemblage; D is the bulk distribution coefficient in the starting assemblage and P is the bulk distribution coefficient of eutectic; f is the degree of partial melting.

Figure 12: Whole-rock CaO vs. MgO diagram of the Ankililoaka lavas and hypothetical primary melts (orange triangles, basanites; red circles, alkali basalts) calculated for them (supplementary Table 12). Black broken arrow is the typical liquid line of descent for primary magmas that crystallize olivine (ol), clinopyroxene (cpx) and plagioclase (plag). Peridotite and pyroxenite partial melt fields after Herzberg & Asimow (2008).

Supplementary Table Captions

Table S1: X-ray fluorescence data of the Ankililoaka samples.

Table S2-S10: compositions of olivine, Cr-spinel, Fe-Ti oxides, clinopyroxene, feldspars, feldspathoids, apatite, mica, amphibole and glass.

Table S11: $^{40}Ar/^{39}Ar$ data for individual aliquots of Ankililoaka groundmass separates.

Table S12: Calculated primary melts composition of the Ankililoaka lavas, using the program of Lee et al. (2009).

Table S13: melting modes, source compositions and partition coefficients used in this paper.

Table S14: Measured and tabulated analyses of international standards.

Supplementary Figure captions

Figure S1: Photomicrographs (plane polarized light) of the Ankililoaka and Late Cretaceous samples: (a-b) Ankililoaka basanites: phenocrysts of olivine (and clinopyroxene in b) in a groundmass with olivine, clinopyroxene, feldspars and magnetite; (c-d) Ankililoaka alkali basalts: olivine phenocrysts and microphenocrysts in a groundmass with plagioclase, clinopyroxene and opaque oxides.

Figure S2: Major oxide and trace element diagrams with the composition of Ankililoaka samples and other Cenozoic mafic Madagascar rocks.

Table 1: Representative bulk-rock analyses of the Ankililoaka samples

sample	M901	M904	M905	M907	M914	M915A	M916	M919	M920	M922	M925	M927
rock name	bsn	bsn	bsn	bsn	bsn	bsn	bsn	bsn	bsn	alk bas	alk bas	alk bas
Lat S	22°27.230'	22°27.808'	22°26.011'	22°42.780'	22°28.891'	22°32.081'	22°31.992'	22°31.838'	22°31.838'	22°31.281'	22°40.690'	22°40.690'
Long E	43°42.861'	43°42.479'	43°43.568'	43°43.729'	43°40.472'	43°39.200'	43°39.291'	43°37.337'	43°37.337'	43°28.669'	43°37.308'	43°37.308'
Analysis method	ICP	ICP	ICP	ICP	ICP	ICP	ICP	ICP	ICP	ICP	ICP	ICP
SiO_2	42.84	42.66	42.78	43.60	42.83	44.09	44.12	42.34	41.05	44.91	46.89	44.18
TiO_2	3.24	3.37	3.57	2.89	2.89	2.32	2.31	2.76	2.82	2.28	2.52	2.61
Al_2O_3	13.51	13.19	13.45	12.74	12.88	13.36	13.50	11.73	11.26	12.07	12.30	12.53
Fe_2O_{3t}	12.99	12.70	13.35	12.33	13.43	11.66	11.32	13.39	13.92	12.74	12.16	13.00
MnO	0.14	0.14	0.15	0.14	0.17	0.14	0.14	0.14	0.19	0.14	0.13	0.18
MgO	7.88	8.64	7.99	9.09	8.12	9.04	9.06	12.05	12.66	10.16	9.47	9.43
CaO	11.13	11.05	10.64	11.25	11.33	11.31	11.43	12.44	12.73	11.91	10.78	10.65
Na_2O	3.52	3.29	3.75	3.46	2.25	3.86	3.71	2.48	2.64	3.18	3.40	3.25
K_2O	2.03	1.92	1.38	1.55	1.91	1.66	1.62	1.37	0.91	1.08	0.77	0.99
P_2O_5	1.06	0.93	1.11	1.01	1.05	0.79	0.80	0.74	0.77	1.00	0.66	0.72
LOI	1.65	1.27	1.87	2.06	3.02	1.92	2.15	1.04	1.41	1.09	1.00	1.64
Be	3	3	3	2	3	3	3	2	2	2	2	2
Sc	20	20	20	23	18	22	22	24	26	24	24	22
V	252	263	268	264	225	213	212	247	259	220	233	213
Cr	190	230	130	320	190	320	310	480	510	310	310	260
Co	45	49	45	46	46	45	43	56	57	50	51	47
Ni	70	100	60	100	110	120	120	240	230	160	160	140
Cu	40	50	40	40	50	50	50	70	60	60	60	30
Zn	130	140	130	120	150	130	130	110	110	130	120	110
Ga	23	23	22	21	23	22	21	17	17	20	20	18
Ge	1	1	1	1	1	1	1	1	1	1	1	1
Rb	52	46	32	33	50	53	50	39	28	33	12	68
Sr	2010	1613	1628	1688	1955	1423	1556	1024	914	1149	796	797
Y	34	30	33	31	32	31	32	22	20	29	23	21
Zr	455	415	469	399	463	364	356	251	227	242	231	230
Nb	101	95	93	86	105	109	103	65	60	68	59	56
Sn	3	3	3	2	3	2	2	2	2	2	2	2
Cs	0.7	0.5	0.6	0.7	0.7	0.7	1.1	-	-	1.0	0.8	0.7
Ba	928	828	838	829	923	1020	1001	618	570	794	558	583
La	120.0	95.8	96.8	94.7	100.0	99.7	99.7	53.6	52.1	94.5	56.8	49.0
Ce	223.0	183.0	190.0	179.0	189.0	177.0	178.0	104.0	102.0	163.0	107.0	91.1
Pr	24.8	20.7	21.7	20.2	21.4	19.3	19.4	12.0	11.9	17.5	11.9	10.5
Nd	92.1	80.0	83.0	75.7	80.8	70.6	71.2	47.4	47.6	62.9	46.2	40.0
Sm	16.8	14.9	15.4	14.4	15.4	13.5	13.8	9.5	9.7	11.4	9.3	8.8
Eu	5.0	4.5	4.7	4.3	4.7	4.1	4.3	2.9	3.1	3.3	2.9	2.8
Gd	12.5	11.3	12.2	11.0	11.6	10.6	10.6	7.8	7.7	8.5	7.7	7.5
Tb	1.7	1.6	1.6	1.5	1.6	1.4	1.5	1.1	1.0	1.2	1.1	1.0
Dy	8.5	7.9	8.3	7.5	7.9	7.6	7.5	5.5	5.2	6.2	6.2	5.7
Ho	1.5	1.3	1.3	1.2	1.3	1.3	1.2	0.9	0.8	1.1	1.0	1.0
Er	3.5	3.1	3.4	3.1	3.1	3.2	3.1	2.2	2.1	2.7	2.5	2.4
Tm	0.44	0.38	0.42	0.41	0.41	0.40	0.39	0.28	0.26	0.35	0.34	0.30
Yb	2.60	2.20	2.30	2.40	2.40	2.40	2.40	1.60	1.50	2.10	2.00	1.70
Lu	0.38	0.33	0.34	0.33	0.32	0.36	0.35	0.24	0.22	0.31	0.28	0.23
Hf	9.0	8.2	8.8	7.6	8.3	7.4	6.9	4.8	4.4	4.6	5.0	5.2
Ta	6.0	5.3	5.5	4.9	5.6	6	5.6	3.3	2.9	3.1	3.2	3.4
W	1.0	-	1.0	-	2.0	2.0	1.0	-	-	2.0	-	-
Pb	7.0	6.0	7.0	5.0	6.0	9.0	9.0	-	-	7.0	-	-
Th	12.2	10	9.9	10	10.2	14.1	13.5	6.0	5.3	12.0	7.5	7.0
U	3.2	2.6	2.7	2.5	2.7	3.5	3.4	1.4	1.2	2.7	1.7	1.7

Major and minor element oxide values are in wt.%; trace element data are in ppm. LOI (weight loss on ignition) was measured gravimetrically.
bsn, basanite; alk bas, alkali basalt.

Table 2: Summary of $^{40}Ar/^{39}Ar$ dating results for the Ankililoaka samples

Sample	Material	Plateau age (Ma, ±2σ)	MSWD	P	Total ^{39}Ar released (%)	Inverse Isochron age (Ma, ±2s)	$^{40}Ar/^{36}Ar$ intercept (±1s)	MSWD isochron
M902	groundmass	12.03±0.09	0.10	1.00	97.6	12.19±0.55	297.2±4.5	0.12
M914	groundmass	10.55±0.06	1.10	0.37	100.0	10.87±0.20	296.1±1.5	0.69
M918	groundmass	11.5±0.11	0.30	1.00	93.9	11.35±1.38	299.6±10.5	0.27

MSWD is mean square weighted deviate and p is the corresponding probability for plateau. Errors are reported at the 2 s confidence level.

Click here to download Table Ankililoaka Tab.3.xls

Table 3: Sr-Nd-Pb isotopic compositions for the Ankililoaka samples

sample	rock type	$^{87}Sr/^{86}Sr$	±2σ internal	$^{87}Sr/^{86}Sr_i$	$^{143}Nd/^{144}Nd$	±2σ internal	$^{143}Nd/^{144}Nd_i$	$^{206}Pb/^{204}Pb$	±2σ internal	$^{207}Pb/^{204}Pb$	±2σ internal	$^{208}Pb/^{204}Pb$	±2σ internal
Ankililoaka													
M901	bsn	0.70359	13	0.70358	0.512804	14	0.512796	19.340	0.0007	15.627	0.0007	39.373	0.0021
M904	bsn	0.70382	9	0.70380	0.512806	12	0.512798	19.337	0.0009	15.633	0.0008	39.389	0.0026
M905	bsn	0.70344	8	0.70343	0.512822	11	0.512814	19.388	0.0009	15.640	0.0008	39.427	0.0024
M907	bsn	0.70348	10	0.70348	0.512792	11	0.512783	19.284	0.0009	15.638	0.0009	39.363	0.0026
M914	bsn	0.70452	17	0.70451	0.512823	16	0.512815	19.227	0.0011	15.613	0.0012	39.238	0.0039
M915A	bsn	0.70368	13	0.70366	0.512802	14	0.512794	19.075	0.0011	15.612	0.0010	39.127	0.0030
M920	bsn	0.70356	13	0.70355	0.512807	13	0.512798	19.079	0.0008	15.615	0.0009	39.108	0.0029
M922	alk bas	0.70384	13	0.70383	0.512819	14	0.512811	18.843	0.0009	15.607	0.0009	38.898	0.0026
M925	alk bas	0.70373	13	0.70373	0.512820	11	0.512812	18.923	0.0009	15.626	0.0008	38.959	0.0025
Std	BHVO-2				0.512985	8	(0.512984 ± 11, Weis *et al*. 2006)						
Std	BHVO-2				0.512974	11	(0.512987 ± 19, long-term UCT average n = 120/exclude 1)						
Std	BHVO-2				0.512976	9	(0.512980 ± 12, GEOREM)						
Std	ref JNdi-1				0.512115	7	(Tanaka *et al*. 2000)						
Std	BHVO-2	0.70349	12		(0.703479 ± 20, Weis *et al*. 2006)								
Std	BHVO-2	0.70345	13		(0.703489 ± 44, long-term UCT average n = 124/exclude 6)								
Std	BHVO-2	0.70347	10		(0.703469 ± 17, GEOREM)								
Std	BHVO-2	0.70347	15										
Std	BHVO-2							18.651	0.0007	15.536	0.0006	38.233	0.0019
Std	BHVO-2							18.692	0.0008	15.538	0.0010	38.260	0.0028
Std	BHVO-2						Weis *et al*. 2006	18.647	0.0242	15.5334	0.0094	38.2367	0.0182
Std	BHVO-2						GEOREM range	18.514-18.687		15.457-15.558		37.992-38.294	
Std	BHVO-2						(long-term UCT average n = 58/exclude 3)	18.631	0.0620	15.534	0.0139	38.224	0.0483
Std	ref NIST-981						Galer & Abouchami 1998	16.941	0.0015	15.496	0.0016	36.722	0.0044

Subscripts “i” on Sr and Nd isotopic ratios indicate initial (age-corrected to 11 Ma) values.
bsn, basanite; alk bas, alkali basalt.

Figure 1

Click here to download Figure Ankililoaka Fig.1.pdf

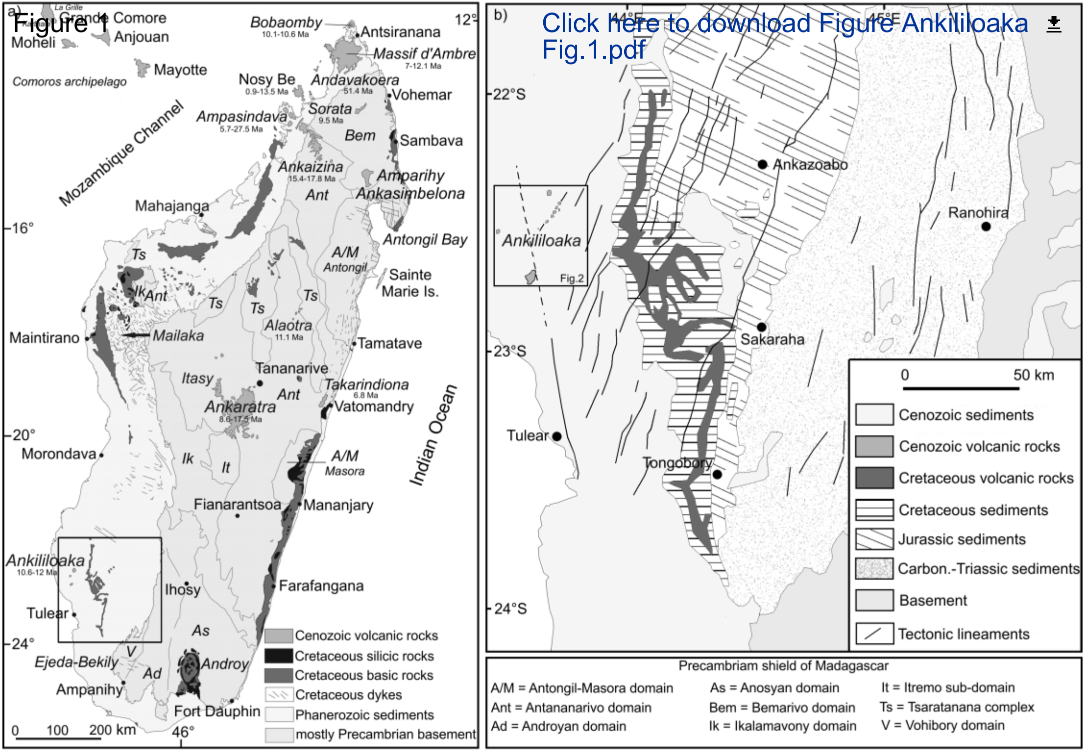

Figure 2

Click here to download Figure Ankililoaka Fig.2.pdf

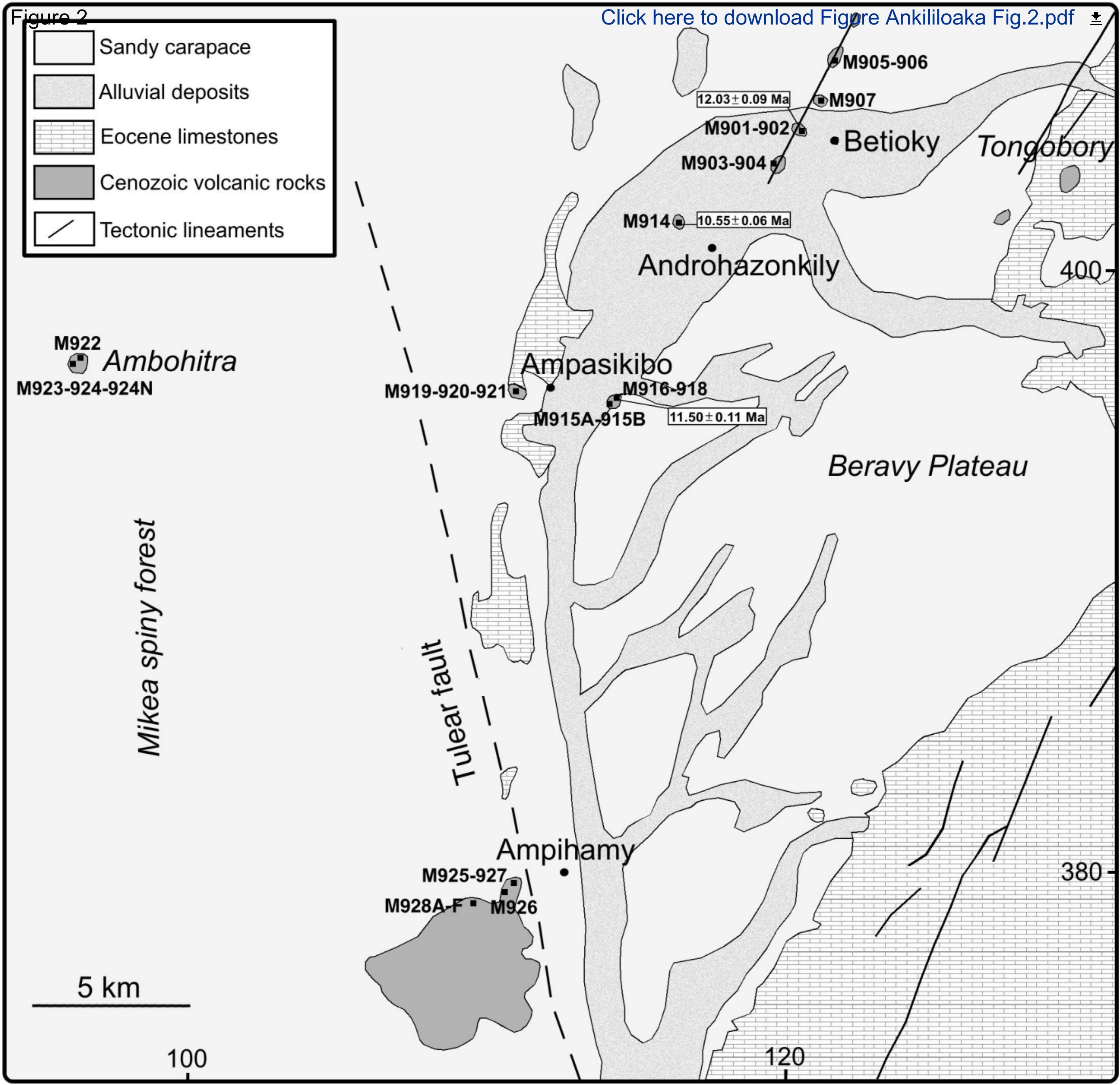

Figure 3

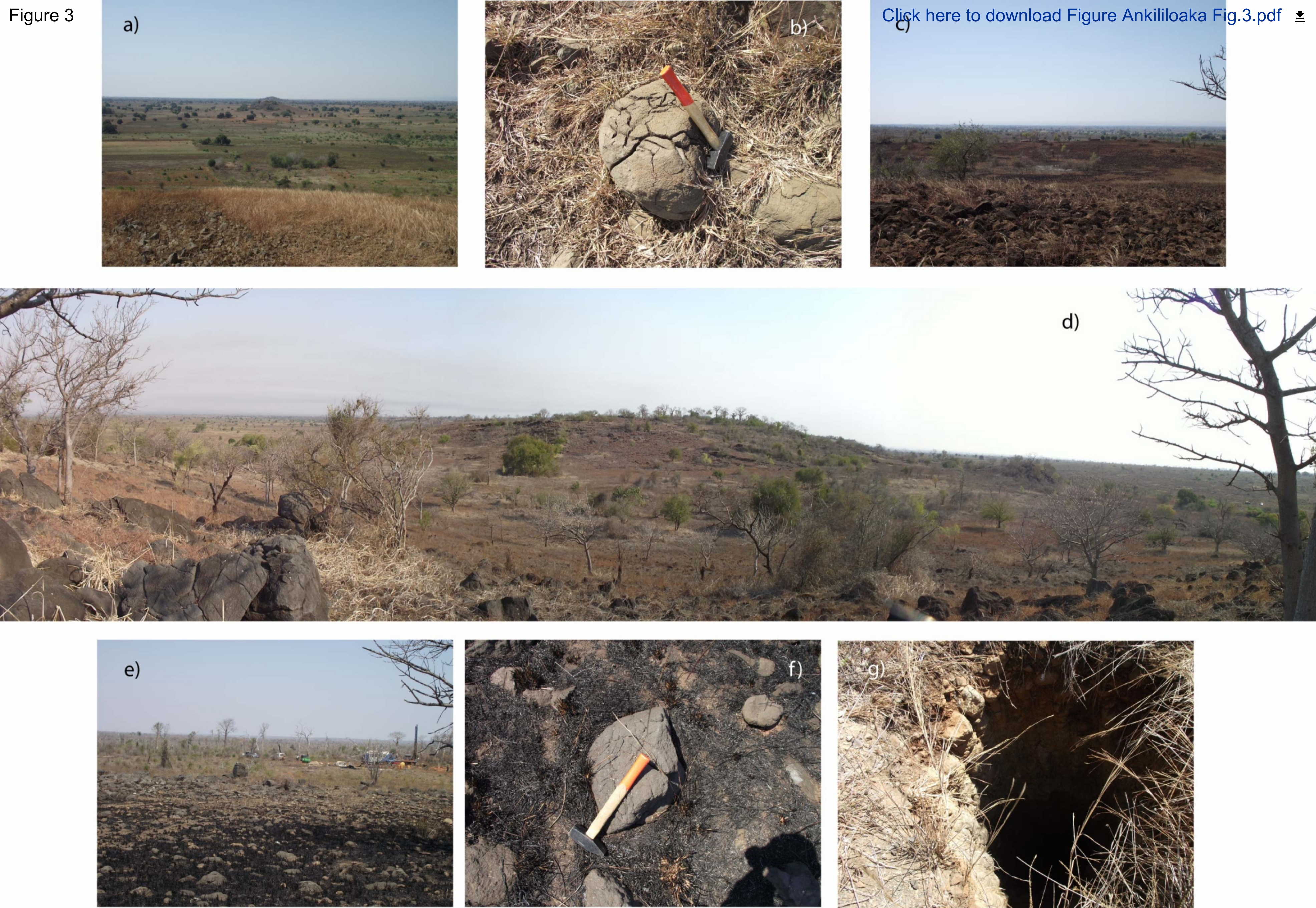

Figure 4

Click here to download Figure Ankililoaka Fig.4.pdf

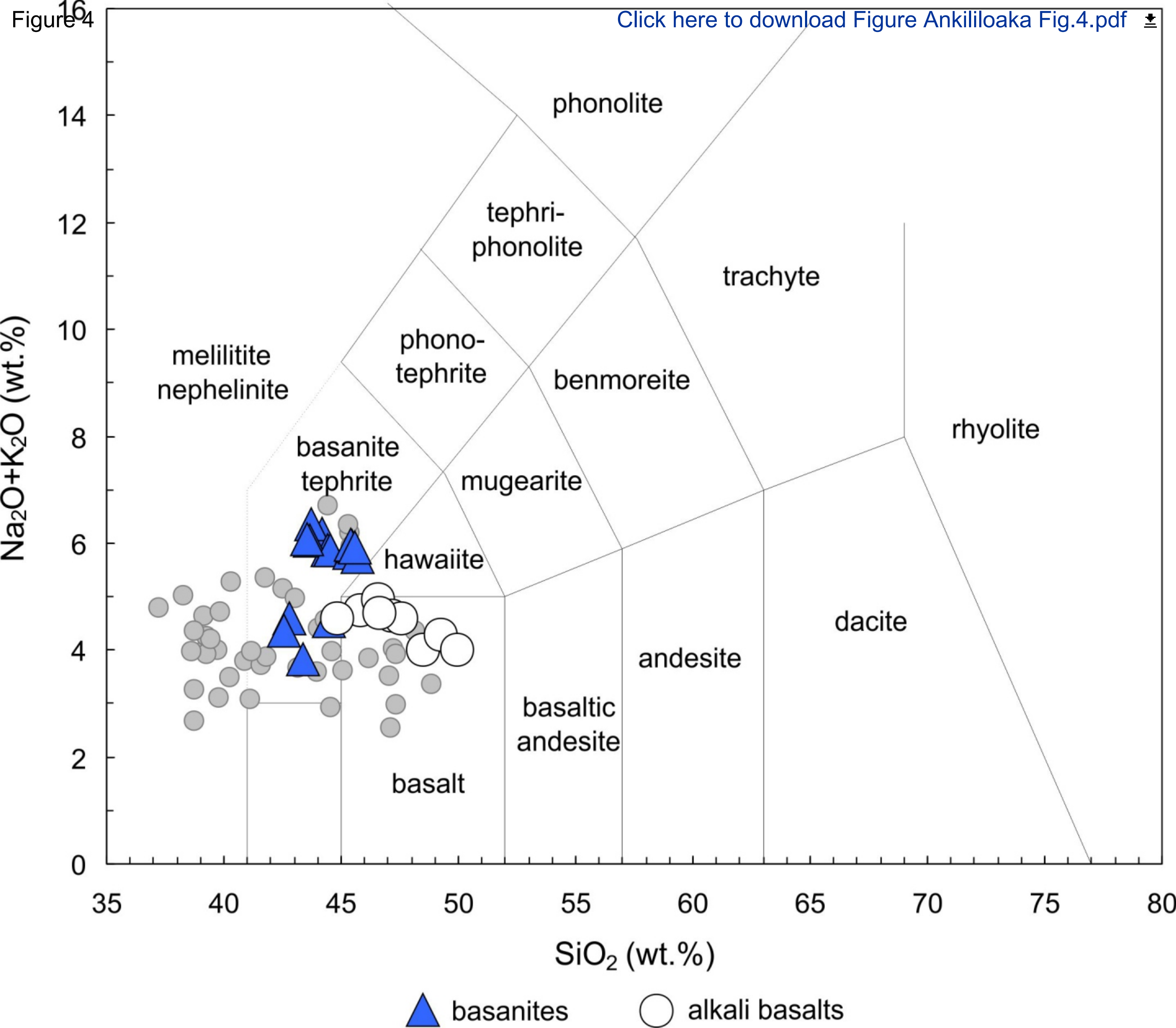

Figure 5

Click here to download Figure Ankililoaka Fig.5.pdf

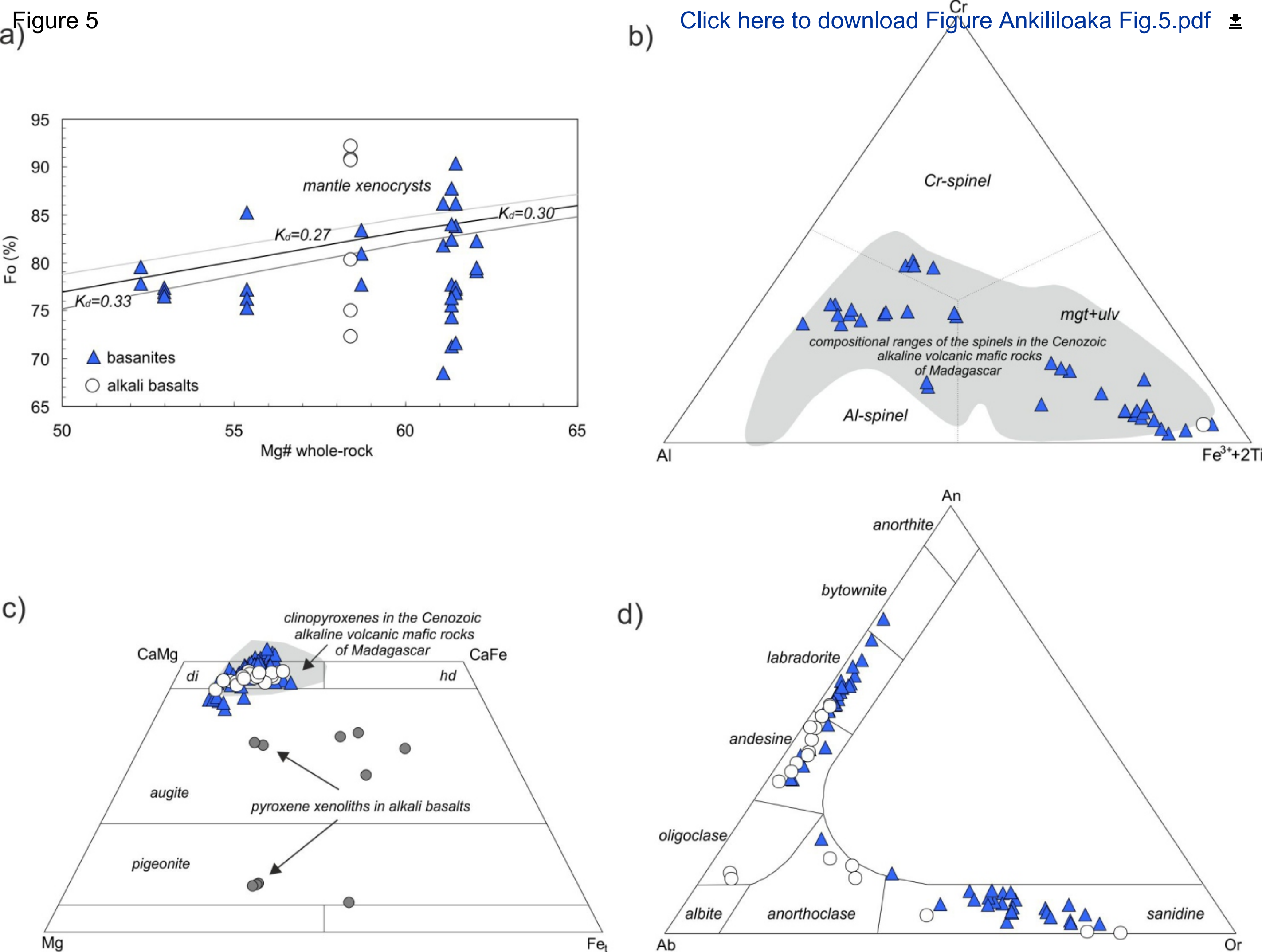

Figure 6

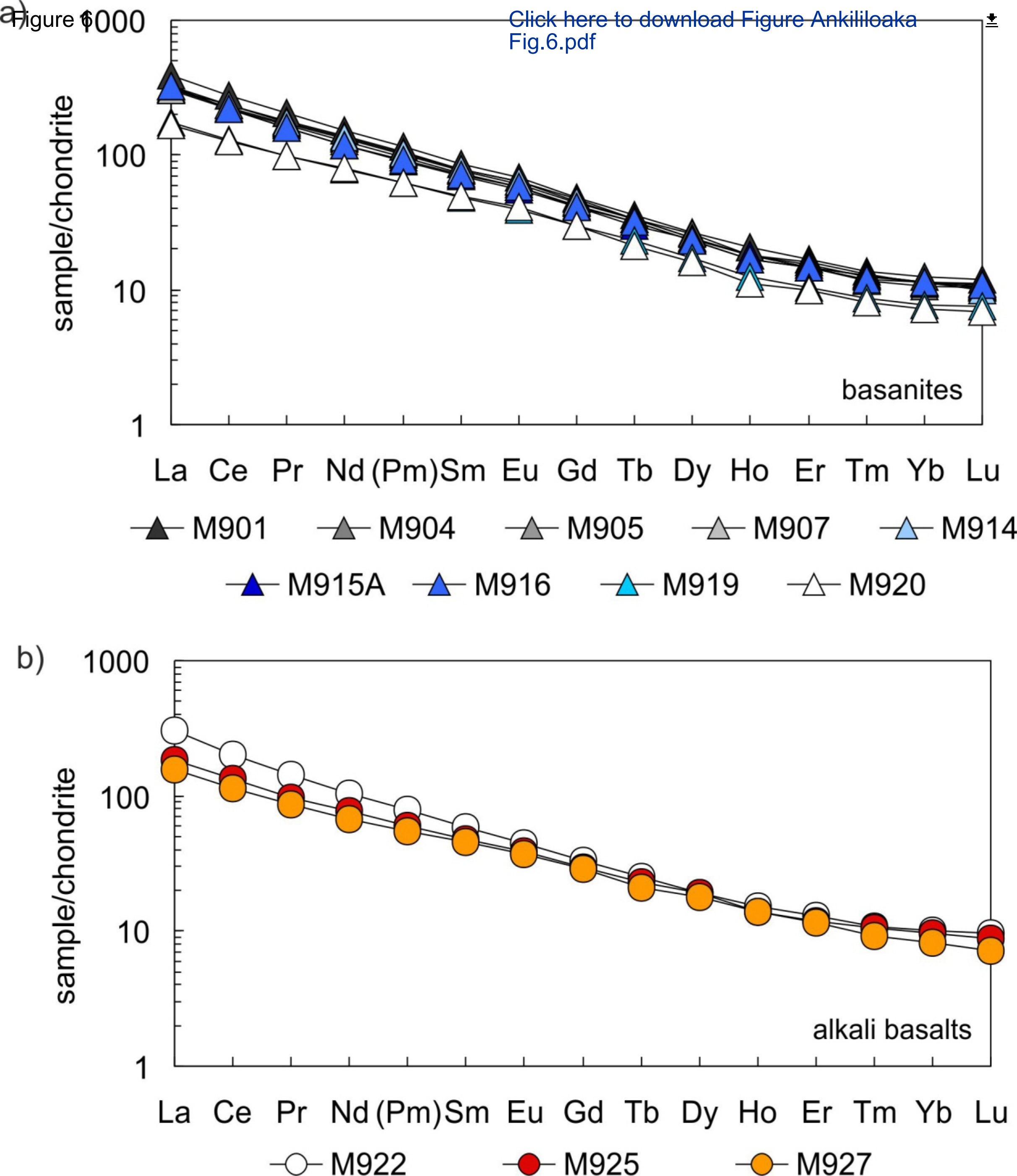
a)
1000
100
10
1
sample/chondrite
basanites
La Ce Pr Nd (Pm) Sm Eu Gd Tb Dy Ho Er Tm Yb Lu
M901
M904
M905
M907
M914
M915A
M916
M919
M920
b)
1000
100
10
1
sample/chondrite
alkali basalts
La Ce Pr Nd (Pm) Sm Eu Gd Tb Dy Ho Er Tm Yb Lu
M922
M925
M927

Figure 7

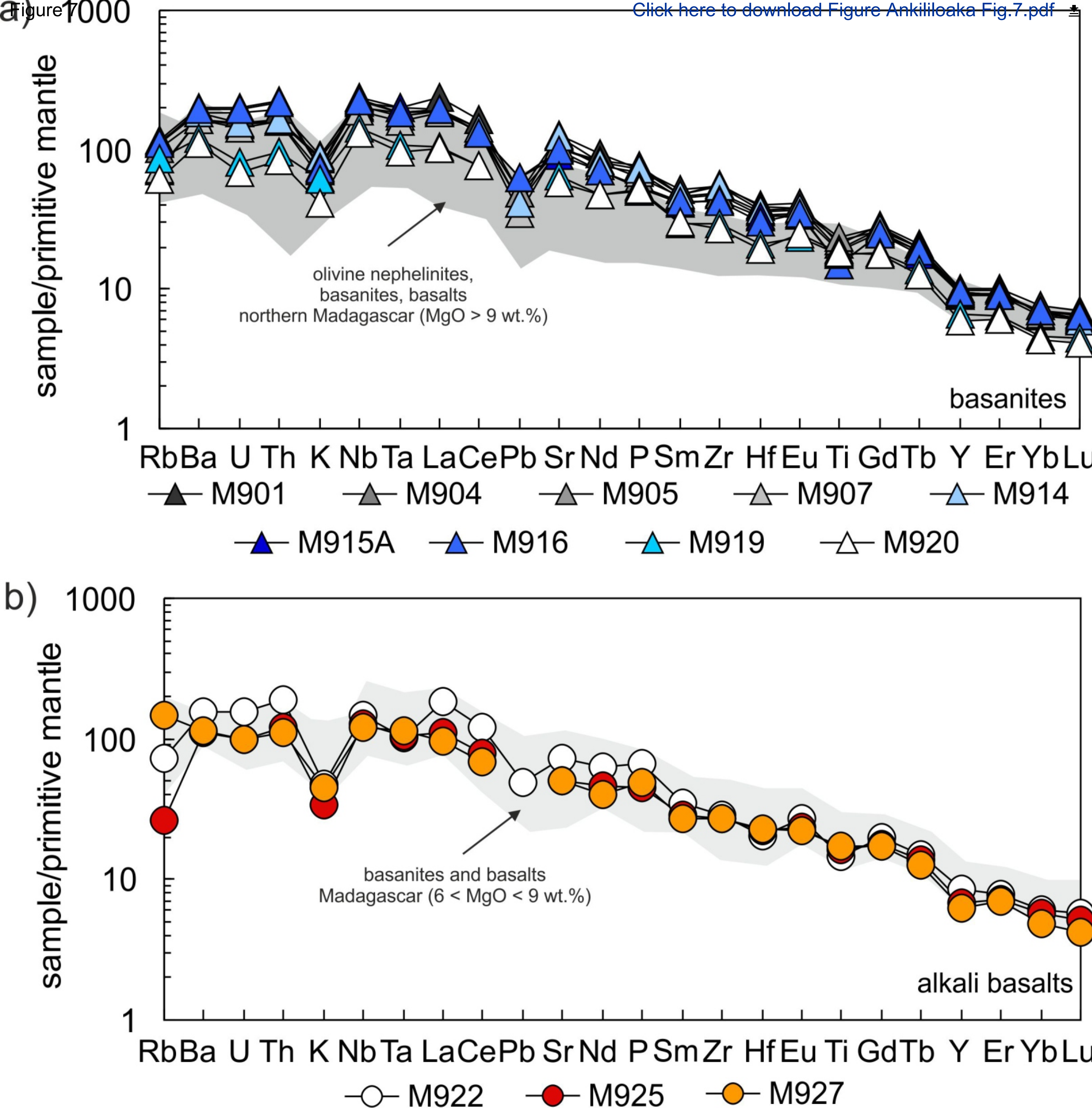
a)
1000
100
10
1
sample/primitive mantle
olivine nephelinites,
basanites, basalts
northern Madagascar (MgO > 9 wt.%)
basanites
Rb Ba U Th K Nb Ta La Ce Pb Sr Nd P Sm Zr Hf Eu Ti Gd Tb Y Er Yb Lu
M901
M904
M905
M907
M914
M915A
M916
M919
M920
b)
1000
100
10
1
sample/primitive mantle
basanites and basalts
Madagascar (6 < MgO < 9 wt.%)
alkali basalts
Rb Ba U Th K Nb Ta La Ce Pb Sr Nd P Sm Zr Hf Eu Ti Gd Tb Y Er Yb Lu
M922
M925
M927

Figure 8

Click here to download Figure Ankililoaka Fig.8.pdf

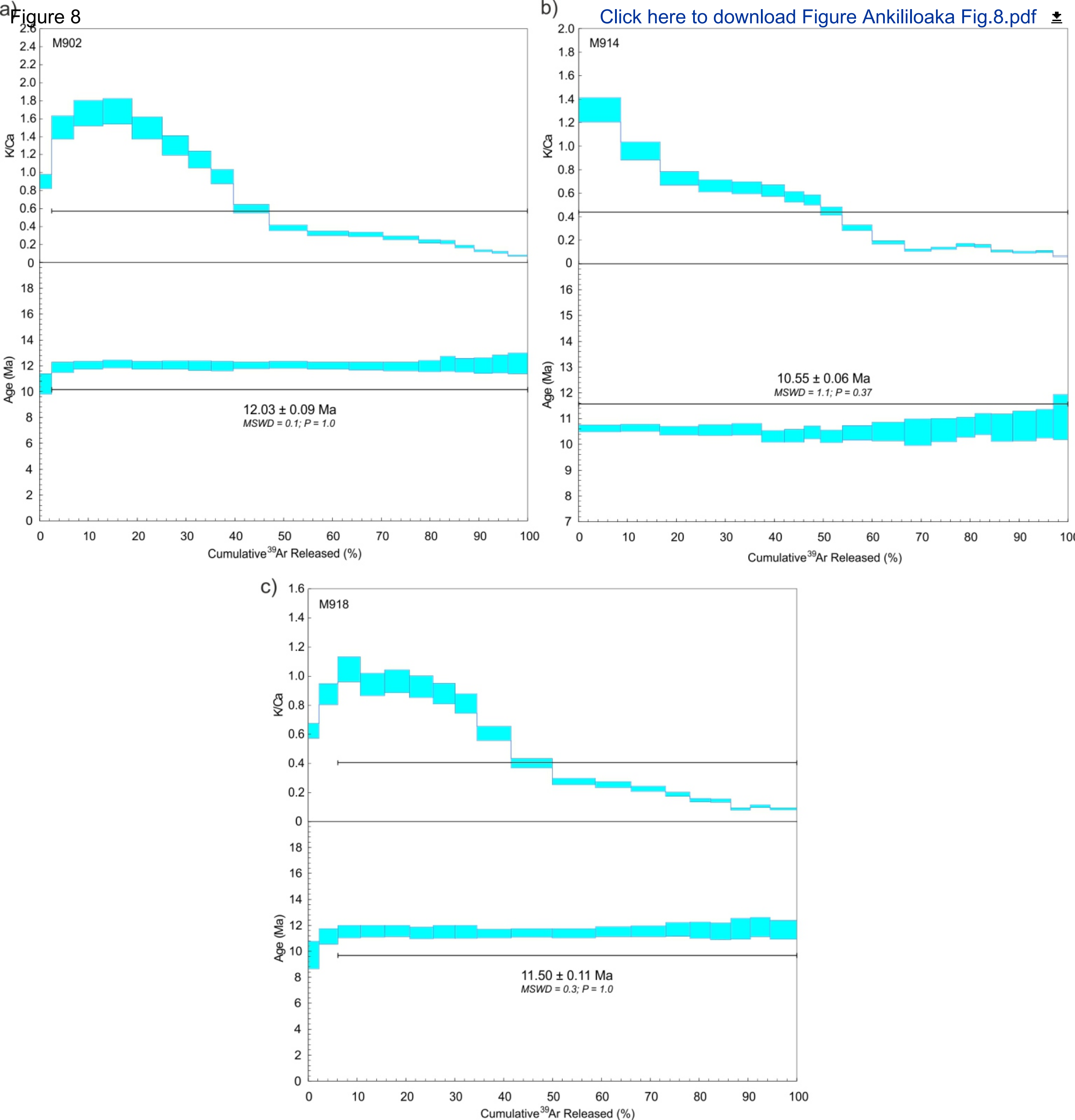

Figure 9

Click here to download Figure Ankililoaka Fig.9.pdf

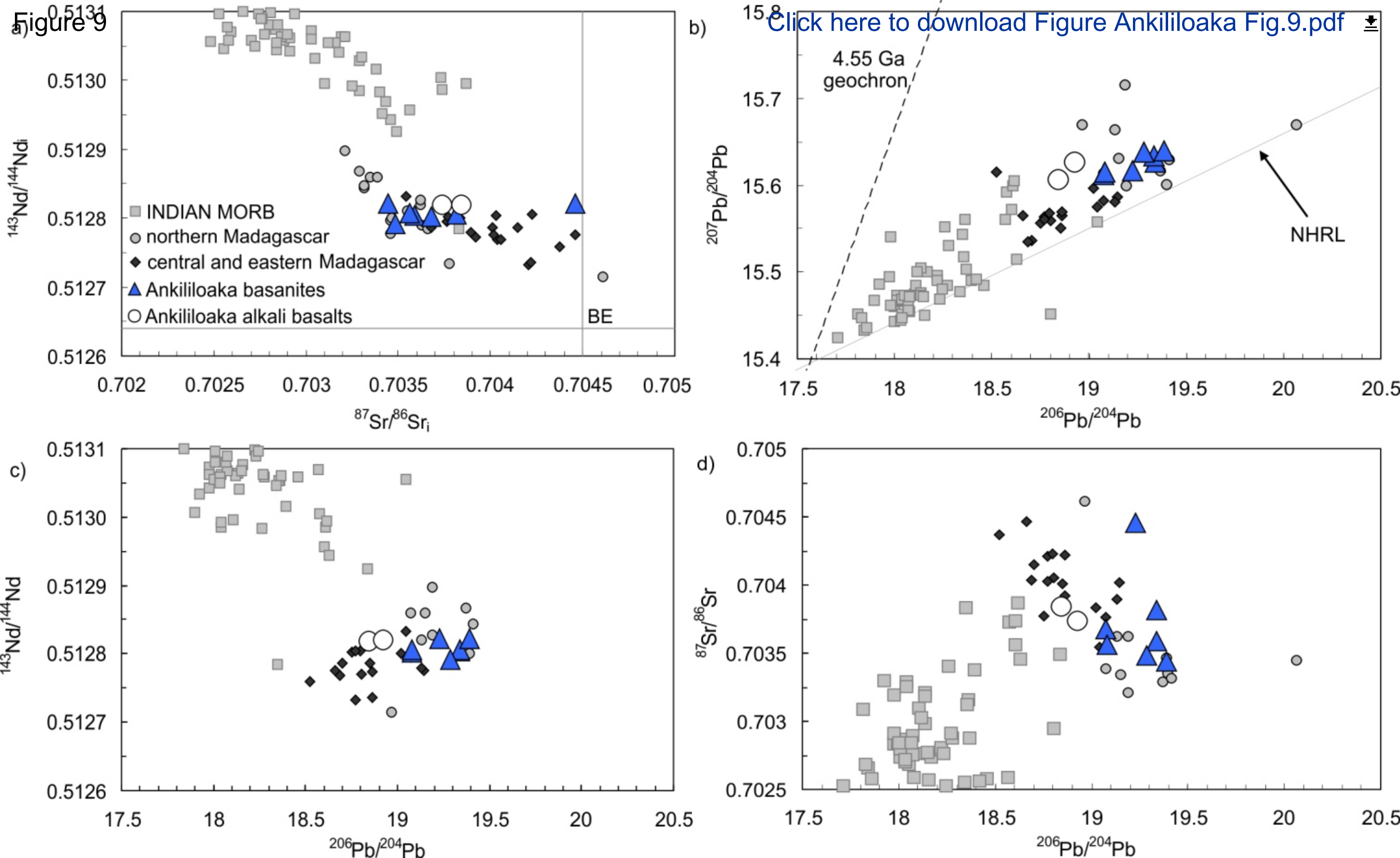

Figure 10

Click here to download Figure Ankililoaka Fig.10.pdf

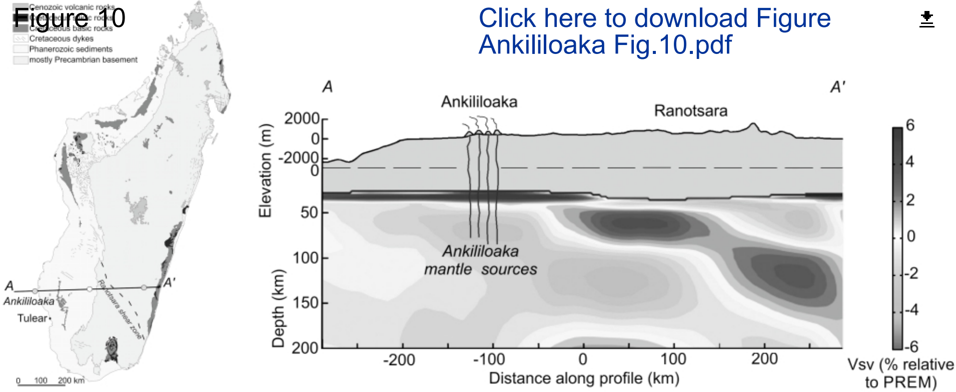

Figure 11

Click here to download Figure Ankililoaka Fig.11.pdf

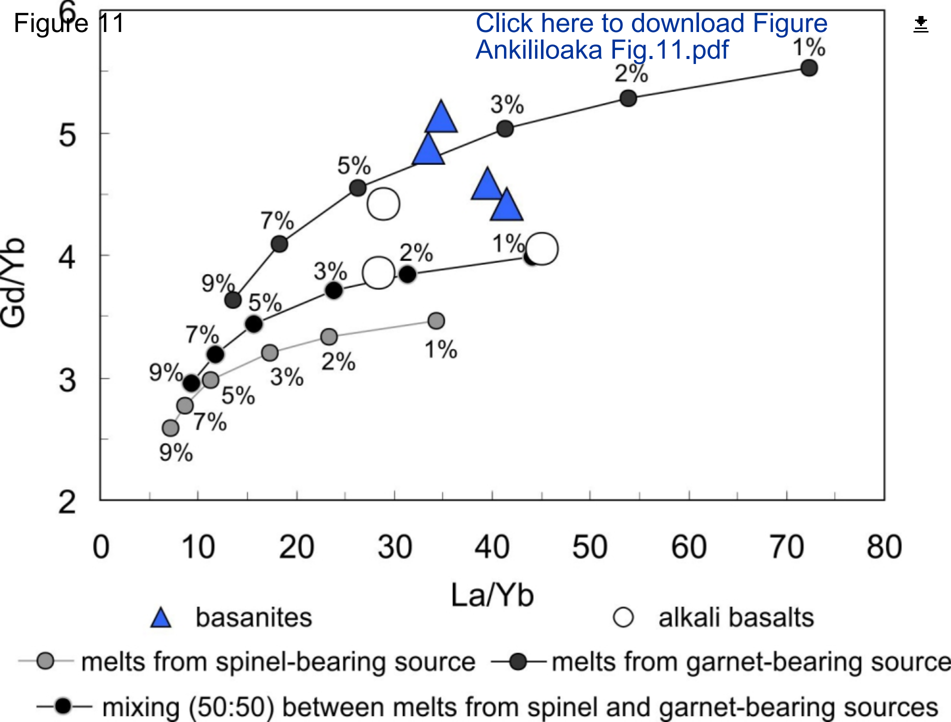

Figure 12

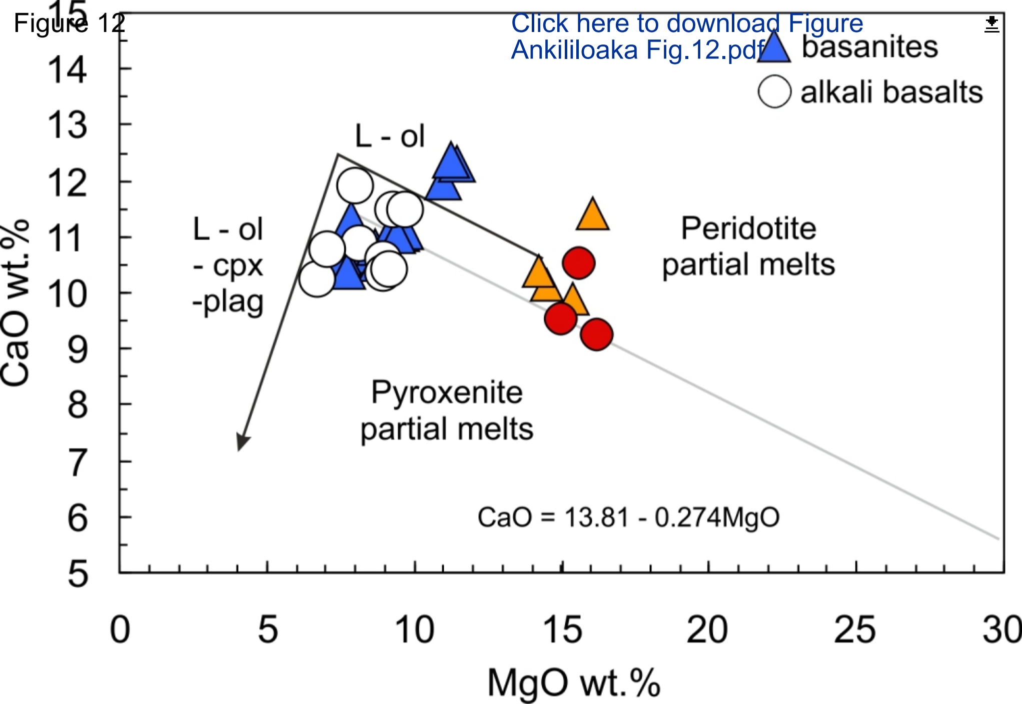
basanites
alkali basalts
L - ol
L - ol
- cpx
-plag
Peridotite
partial melts
Pyroxenite
partial melts
CaO = 13.81 - 0.274MgO
CaO wt.%
MgO wt.%
5
6
7
8
9
10
11
12
13
14
15
0
5
10
15
20
25
30

Supplementary material (Fig.2)

Click here to access/download
Supplementary material (not datasets)
Ankililoaka supplementary Fig.2.pdf

Supplementary material (Fig.2cont)

Click here to access/download
Supplementary material (not datasets)
Ankililoaka supplementary Fig.2 cont..pdf

Supplementary material (supplementary Tables)

Click here to access/download
Supplementary material (not datasets)
Ankililoaka supplementary Tables.xls